Construction and Building Materials 328 (2022) 127114

Contents lists available at ScienceDirect

Construction and Building Materials

journal homepage: www.elsevier.com/locate/conbuildmat

Rheological properties and compressive strength of construction and demolition waste-based geopolymer mortars for 3D-Printing

Huseyin Ilcan [a,b], Oguzhan Sahin [a,c], Anil Kul [a,b], Gurkan Yildirim [b,d,*], Mustafa Sahmaran [b]

[a] Institute of Science, Hacettepe University, Beytepe, Ankara, Turkey
[b] Department of Civil Engineering, Hacettepe University, Beytepe, Ankara, Turkey
[c] Department of Civil Engineering, Kırşehir Ahi Evran University, Kırşehir, Turkey
[d] Department of Civil and Structural Engineering, University of Bradford, Bradford, United Kingdom

ARTICLE INFO

Keywords:
Geopolymer
Mortar
Construction and demolition waste (CDW)
3-dimensional additive manufacturing (3D-AM)
Rheology
Alkaline activator

ABSTRACT

Entirely construction and demolition waste (CDW)-based ambient-cured geopolymer mortars with rheological properties fitted for 3-dimensional additive manufacturing (3D-AM) were developed in an effort to combine the advantages of improved waste minimization, development of green materials and easy/fast/accurate materials production/processing. CDW-based hollow brick (HB), red clay brick (RCB), roof tile (RT), concrete rubble (C), and glass (G) were used for the development of geopolymer binders while C was used solely as fine aggregates. Mixtures were activated by different combinations of sodium hydroxide (NaOH), calcium hydroxide ($Ca(OH)_2$), and sodium silicate (Na_2SiO_3) as the alkaline activators. Rheological assessments were made based on the empirical test methods including flow table, vane shear and modified mini-slump tests. Compressive strength measurements were also made. Finally, two representative mortar mixtures with low and high viscosity were printed via a laboratory-scale 3D printer and the rheological properties were correlated with printing behavior of geopolymer mortars. Overall, the study showed that entirely CDW-based geopolymer mortars without any chemical admixtures having suitable rheological properties for 3D-AM can be manufactured successfully. The empirical test methods utilized are adequate in determining the rheological properties of CDW-based geopolymer mortars suited for use in 3D-AM. The designed entirely CDW-based geopolymer mortars with adequate compressive strengths were shown to be capable of extrusion via 3D-AM free of any defects/discontinuity, capable of maintaining its initial shape under the effect of the weight of consecutive upper layers and fully matched with the designed printed structure.

1. Introduction

Construction activity-related overexploitation of natural resources (*e.g.*, high levels of concrete production, extraction of raw materials, landfilling of wastes) and greenhouse-gas emissions are among the major problems contributing to environmental degradation and climate change. In this regard, huge amounts of conventional concrete produced can be considered very important as the material constitutes ingredients like Portland cement (PC) and aggregates, acquirement/production of which is quite troublesome economy-/environment-/health-wise. In this regard, PC manufacture is of great importance since it is a very energy-intensive and carbon-emissive process requiring huge amounts of natural raw materials (*e.g.*, limestone, clay, gypsum) together with fossil fuels to be burnt. PC production alone is held responsible for up to 9% of man-made CO_2 emissions globally [1] with a ratio higher than 900 gr CO_2 per kg of PC [2].

Meanwhile, as the countries' infrastructure crumbles, the construction and demolition waste (CDW) industry has become one of the main sectors contributing to the global solid waste production. In EU, CDW is the largest waste stream, by volume accounting for one-third of all the waste produced. In 2017, the amount of CDW only in the USA was approximately 569.4 Mt and the amount of CDW generated from demolition processes was nearly 94% [3]. In China, the annual rate of increment in CDW production is estimated to be in billions in the forthcoming years [4]. In the following 20 years, Turkey will demolish/reconstruct 8.2 M structures (nearly 21% of its total registered building stock) following the new infrastructural transformation action plan [5]. Examples clearly point out for the seriousness of the CDW issue on a

* Corresponding author.
E-mail address: gurkanyildirim@hacettepe.edu.tr (G. Yildirim).

https://doi.org/10.1016/j.conbuildmat.2022.127114
Received 3 January 2022; Received in revised form 28 February 2022; Accepted 9 March 2022
Available online 14 March 2022

global scale and therefore, tackling CDW properly is critical, and prolonged sustainability requires the production of eco-friendly construction materials.

Considering the undeniable negative effects of PC production, latest research efforts are being increasingly concentrated on the development of greener binders. In this regard, geopolymers are potential alternatives of PC for the realization of binder materials with less energy requirement and CO_2 emission. Produced by the reaction between aluminosilicate precursors (*e.g.*, blast furnace slag, fly ash, calcined clays, natural pozzolans) and alkaline activators (*e.g.*, sodium hydroxide, potassium hydroxide, calcium hydroxide, sodium silicate), geopolymers have been gaining significant attention from construction industry in recent years [6,7]. The abovementioned mainstream precursors, which are mainly used to produce geopolymers in literature, are highly demanded by the PC and concrete industry at costs higher than and/or comparable to PC given their proven performance and successful use as supplementary cementitious materials [8]. In addition, these precursors may necessitate high transportation costs, pre-treatment and not even be available for a certain area of interest, where geopolymers are planned to be manufactured at the first place. It is therefore critical to find alternative source materials (*i.e.*, precursors) compatible to be used in geopolymer production for an easier and widespread production/application. Considering the fact that CDW generation is ubiquitous in the world and CDW is mainly landfilled in the clean areas and/or used for low-tech applications (*e.g.*, non-structural road base/sub-base filling), CDW-based materials (*e.g.*, concrete, bricks, tiles, ceramics, glass) can be used in producing geopolymers for the sake of effective, innovative and high-grade waste valorization. Recent works of the authors have presented a detailed literature review focusing on the utilization of CDW-based materials in geopolymer paste production [8,9].

Along with the material-related breakthroughs, operation-related breakthroughs utilizing advanced manufacturing technologies need to be made to achieve truly sustainable construction practices. In this regard, 3-dimensional additive manufacturing (3D-AM), which is defined as the layer-by-layer deposition, is a new generation sustainable method of construction attracting considerable interest recently thanks to its significant advantages over traditional techniques including increased geometrical design flexibility, cost efficiency, fast construction speed, low labor requirement and labor-related mistakes, formwork freedom lower potential of waste generation in practice and others [10–14]. For satisfactory 3D-AM applications, material designed to be printed needs to have certain fresh-state properties including; mixtures must (i) be extrudable to be easily transferred/evacuated, (ii) be buildable to withstand the pressure from its own and consecutive upper layers without losing its shape and (iii) have adequate open-time to be printed during a certain period.

In a number of research studies, geopolymer technology merged into 3D-AM technology has been of focus. Panda et al. [15] developed a 3D-printable geopolymer mortar by using fly ash (FA), ground granulated blast-furnace slag (GGBS) and silica fume (SF) as aluminosilicate precursors with potassium hydroxide and potassium silicate as the alkaline activators. A printable thixotropic zone (an interval for yield stress) for 3D-printability (in terms of extrudability and buildability) was specified in the study. Moreover, it was revealed that the minimum threshold limit level of 10,000 (which is specified by the area of hysteresis loop between the up and down curve of torque-speed graph obtained from rheometer test) was required for the thixotropic behavior of the mixtures suitable for 3D-printing application although this limit level can vary according to some points/parameters (*e.g.,* test equipment, mixture design and shear rate applied by the rheometer). In another study, Panda et al. [16] examined the effects of the different operational parameters (*e.g.,* print speed, printing time gap between layers, nozzle standoff distance) on the tensile bond strength of 3D printed geopolymer mortars produced by using FA, GGBS and SF as aluminosilicate precursors, potassium silicate as the alkaline activator and river sand (with the maximum particle size [D_{max}] of 1.15) as the fine aggregates. Bingham parameters (yield stress and plastic viscosity) of the geopolymer mortars were measured by using a rheometer for every 5-minute intervals and the mixture's open-time was determined to be 20 min. It was also concluded in this study that higher printing time gap between consecutive layers decreased the bond strength while lower printing speed and nozzle standoff distance resulted in higher bond strength results. Panda et al. [17] examined the effect of mixture design on the fresh and hardened properties of geopolymer mixtures containing different amounts of FA, GGBS and SF as aluminosilicate precursors and blend of sodium silicate and NaOH as alkaline reagent. The rheological properties of geopolymer mixtures (thixotropy and buildability) after different resting times were evaluated by using a rheometer under different implementation protocols. It was stated that geopolymer do not have thixotropic behavior compared to ordinary PC-based mixtures due to the absence of colloidal interaction. Similar statement was also made in other studies [18–22]. Annapareddy et al. [20] worked on the fresh and hardened properties of cementitious materials including ordinary PC-mortar (PC + recycled glass aggregate) and geopolymer mortar (FA, GGBS and SF + potassium silicate + recycled glass aggregate). Rheological properties of these mortars were compared by performing viscosity recovery tests by a rheometer, slump measurements and visual inspections on the freshly printed materials and it was concluded that PC-based binder showed preferable thixotropy recovery behavior compared to geopolymer most probably due to the absence of colloidal interaction available in the geopolymer. Nematollahi et al. [23] investigated the fresh and hardened properties of geopolymer mortars (FA + $NaOH/Na_2SiO_3$ + silica sand) with various contents of polypropylene fiber. For testing the rheological response of the mixtures, testing methods including visual inspection, flow table (dynamic agitation) and shape retention ability (static loading) were utilized. It was concluded that the threshold for optimum workability of mixtures for 3D-printing as a result of the flow table test including 25 drops of the flow table was 134–158 mm. It was also observed that there were incontrovertible directional variations on the hardened properties of the printed structures. Incorporation of fiber into the mixtures enhanced the shape retention ability, compressive strength in the perpendicular directions, deformation capacity and fracture energy while decreasing the interlayer bond strength beyond a certain level. Bong et al. [24] performed a study to develop 3D-printable geopolymer mortars (FA/GGBS + [Na_2SiO_3 (two different types)/NaOH or K_2OSi_3/KOH] + sand) subjected to ambient curing and focused on the effects of different parameters including the type of alkaline activator, ratio of silicate-to-hydroxide solution and viscosity of silicate solutions on the fresh and hardened properties of the mortar mixtures. Extrudability, buildability and open-time of the mixtures were evaluated by the time-dependent visual and dimensional inspections after printing. According to the results, the type of alkaline activator solution and SiO_2/Na_2O ratio of the Na_2SiO_3 solution were considerably influential on the open-time and buildability of the mixtures. It was reported that the lower SiO_2/Na_2O ratio of the Na_2SiO_3 solution leads to longer setting time/open-time due to lower rate of geopolymerization reactions. The higher ratio of silicate-to-hydroxide solutions resulted in slower geopolymerization reactions and thereby relatively longer open-time. It was also concluded that the rate of the geopolymerization reactions was influential on the shape retention ability of the geopolymer mortars. Kashani and Ngo [25] investigated the effect of material-/operation-related parameters on the 3D printability of geopolymers (FA, GGBS and SF + sodium *meta*-silicate powder). Rheology and open-time of the mixtures were investigated by performing time-dependent tests with rheometer and Vicat needle, respectively. The study concluded that a balance among mechanisms being influential on the open-time, initial yield stress and time-dependent variability of rheology should be ensured to develop a geopolymers properly fit for 3D-AM applications. Panda et al. [26] investigated the effect of material-related parameters (*i.e.,* water-to-solid ratio, activator-to-binder ratio, addition of nanoclay, molar ratio of activator) on the fresh-state/rheological properties of geopolymer

nanocomposites (FA/GGBS + potassium hydroxide/potassium silicate + river sand [D_{max}: 2 mm] + nanoclay for some mixtures) to assess the extrudability and buildability performances of the mixtures alongside with their shape retention ability and buildability aspects. According to the results, increase in the molar ratio of activators, and decrease in the activator-to-binder/water-to-solid ratios increased the viscosity and yield stress of the mixtures. Addition of nanoclay into the geopolymer mixtures was found to lead to improved ability to recover the thixotropic behavior of the mixtures. With the purpose of developing a printable one-part geopolymer mixture having lower environmental impact, Panda et al. [27] have performed a study, which utilized the same testing procedures on geopolymer mortars (FA/GGBS + potassium hydroxide/potassium silicate + river sand [D_{max}: 2 mm]) manufactured in the work of Panda et al. [26] to evaluate the fresh properties of the mixtures. Visual and dimensional inspections after printing were also other methods used for determining the printability performance of the mixtures. In addition, direction-dependent mechanical tests were performed on the 3D-printed specimens. According to the results of this study, increasing the GGBS content of the geopolymer mixtures led mixtures to have higher yield stress, thixotropy and mechanical strength. It was shown that the printed geopolymer specimens had anisotropic mechanical properties due to their layered structure. In addition to the studies briefly discussed above, further studies positioned especially on the mechanical performance of 3D-printable geopolymer mixtures containing main-stream precursors can be found in the open literature [28–37].

To the best of authors' knowledge, in literature, there are no studies, which focus on the novel aspects of combined use of 100% CDW-based geopolymer mortars and 3D-AM technology, excluding the recent work of the authors, where geopolymer binders with CDW-based precursors were manufactured suitable for 3D-AM applications [38]. Given the scarcity of the subject and for the achievement of truly sustainable construction practices both at the material and operational levels, recently published work of the authors has been taken one step further herein. Different from Şahin et al. [38], in the current study, CDW-based geopolymers were incorporated with CDW-based fine recycled concrete aggregates to obtain geopolymer mortars with fresh properties fitted for 3D printability. By doing so, the ratio of CDW utilization was significantly increased, which is highly beneficial for the sake of enhanced waste upcycling through effective/innovative ways. Different CDW-based materials used for the study were the wastes of hollow brick (HB), red clay brick (RCB), roof tile (RT), glass (G) and concrete rubble (C). For the alkaline activation of geopolymers, sodium hydroxide (NaOH), sodium silicate (Na_2SiO_3) and calcium hydroxide ($Ca(OH)_2$) were used either singly or in binary/ternary combinations. The alkali content of the mixtures was manipulated by modifying the ratio of use of these activators and the effect of the alkaline activator content/combination on both fresh and hardened-state properties of ambient-cured geopolymer mortars was evaluated. Besides, the influence of recycled aggregate on the rheological properties and compressive strength of the CDW-based systems were also investigated. Finally, the performance of selected geopolymer mortar mixtures with the properties fitted for 3D-printability was validated via laboratory-scale 3D-AM applications.

2. Experimental program

2.1. Materials

CDW-based materials (hollow brick [HB], red clay brick [RCB], roof tile [RT], glass [G] and concrete rubble [C]) used in this study were obtained in the assorted form as a result of the selective demolishment practices performed in Turkey. After the initial acquirement, CDW-based materials were reduced in size with the help of jaw crusher and milled separately in laboratory-type ball mill for an hour to obtain powdery materials. The photographs of CDW-based materials right after the initial collection and ball milling are shown in Fig. 1. At the end of the milling process, oxide compositions (Table 1) and particle size distributions (Fig. 2) of the CDW-based precursors were determined by performing X-ray fluorescence analysis (XRF) using wavelength of 0.1–50 Å and laser diffraction analysis having particle size range sensitivity of 0.02–2000 μm, respectively. A true representative specimen of each powdery material was taken from the different portions of the powder batches and oven-dried before the analysis. XRF results indicated that the major oxides available in the chemical composition of the clay-originated precursors (RCB, RT, and HB) were SiO_2, Al_2O_3 and Fe_2O_3, which are fundamentally important oxides for the geopolymerization reactions [39–42]. Different from the clay-originated precursors, the main oxides of C and G were SiO_2, Na_2O and CaO.

As can be seen from Fig. 2, there are certain differences in the grain size distributions of CDW-based precursors, although an identical milling procedure and period were followed for all the materials. The grain

Table 1
Oxide compositions and specific gravity of CDW-based materials.

Oxides, %	HB	RCB	RT	G	C
SiO_2	39.7	41.7	42.6	66.5	31.6
Al_2O_3	13.8	17.3	15.0	0.9	4.8
Fe_2O_3	11.8	11.3	11.6	0.3	3.5
CaO	11.6	7.7	10.7	10.0	31.3
Na_2O	1.5	1.2	1.6	13.6	0.45
MgO	6.5	6.5	6.3	3.9	5.1
SO_3	3.4	1.4	0.7	0.2	0.9
K_2O	1.6	2.7	1.6	0.2	0.7
TiO_2	1.7	1.6	1.8	0.1	0.2
P_2O_5	0.3	0.3	0.3	0.0	0.1
Cr_2O_3	0.1	0.1	0.1	0.0	0.1
Mn_2O_3	0.2	0.2	0.2	0.0	0.1
Loss on ignition	7.8	8.0	7.5	4.3	21.1
Specific gravity	2.89	2.81	2.88	2.51	2.68

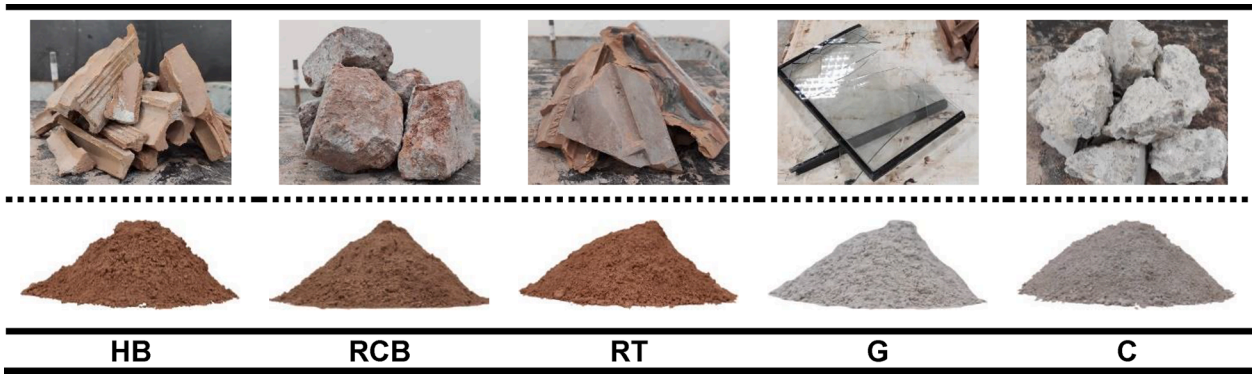

Fig. 1. Digital camera images of the CDW-based precursors after initial collection (top) and ball milling (bottom).

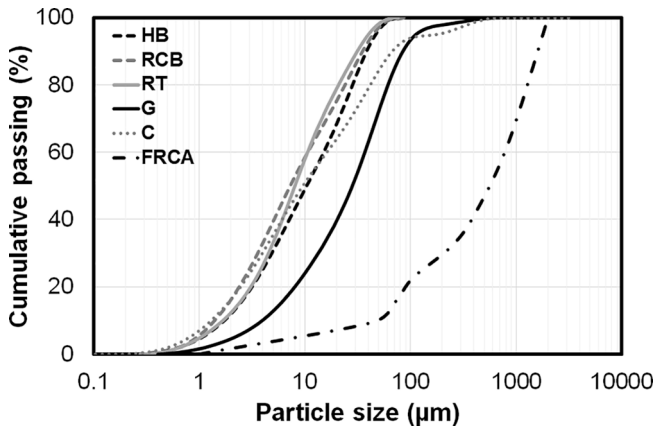

Fig. 2. Particle size distribution curves of CDW-based precursors and fine recycled concrete aggregates (FRCA).

size distributions of RT and RCB were similar to each other, while HB was slightly coarser than them. C was coarser than clay-originated precursors (RCB, RT, and HB). G was the coarsest among all the milled CDW-based materials, yet 70% of its particles was still finer than 45 μm. Differences in the grain size distributions of the materials were expected due to natural differences in the properties of raw materials such as density, hardness, pore structure, etc. Considering the fact that it is difficult, impractical, energy-intensive and cost-inefficient to bring each one of the CDW-based materials into similar particle ranges, no additional steps were taken to change/modify the particles size distributions. This was also done for the possible future studies, which are likely to focus on collective milling of different types of CDW-based materials to better simulate the real-time field conditions, where such wastes are obtained altogether following the construction and demolition applications. In Fig. 3, X-ray diffractograms of the precursors, which were obtained as a result of the X-ray diffraction (XRD) analyses performed by using powder samples, are shown. XRD analyses were carried out with a scan range (2θ) of 5–55° and an increment of 0.02° to identify and characterize the mineral/crystalline phases of the precursors. In Table 2, crystalline phases detected for different CDW-based precursors are shown with the details including the symbol, particle diffraction file (PDF) numbers and chemical formula of the phases. Clay-originated precursors (HB, RCB and RT) had similar XRD patterns containing amorphous to semi crystalline phases. The major crystalline peak of RCB, RT and HB with the highest intensity belonged to quartz phase with the peak mainly centered around 2θ of 27-29°. Diopside, mullite, crystobalite and akermanite were also detected at minor quantities in clay-originated CDW-based precursors depending on the type. For C, the major peaks detected were quartz, diopside and calcite with minor peaks of muscovite and foshagite. Without any identifying crystalline peak, G was amorphous in nature, which was represented by a broad hump

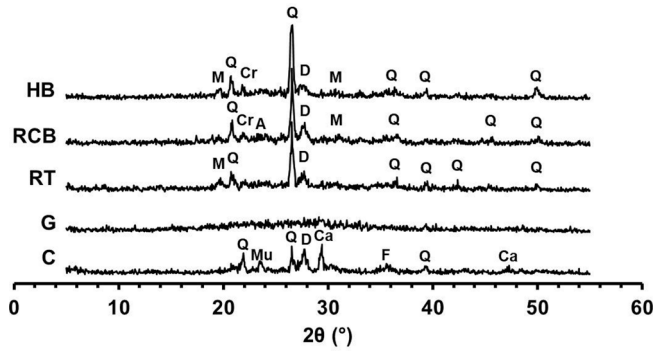

Fig. 3. XRD patterns of CDW-based precursors.

Table 2
Chemical formulations and PDF numbers of crystalline phases in accordance with XRD analyses.

Crystalline phase	Symbol	PDF number	Chemical formula
Quartz	Q	96–101-1160	SiO_2
Crystobalite	Cr	96–900-8230	SiO_2
Diopside	D	96–900-5280	$Al_{0.6}CaMg_{0.7}O_6Si_{1.7}$
Mullite	M	96–900-5502	Al_2O_5Si
Akermanite	A	96–900-6115	$AlCa_2Mg_{0.4}O_7Si_{1.5}$
Calcite	Ca	96–900-9668	$CaCO_3$
Muscovite	Mu	96–101-1050	$Al_3H_2KO_{12}Si_3$
Foshagite	F	96–901-1044	$Ca_4H_2O_{11}Si_3$

centered around 2θ of 28°.

In order to manufacture the mortar mixtures, geopolymers were incorporated with fine recycled aggregates obtained from CDW-based concrete rubble (C), which was also used in the mixture designs of geopolymers partly as will be presented in the following section. The maximum aggregate size of the FRCA was limited to around 2 mm to prevent possible blockage and transportation problems endangering the 3D-AM process by taking the particle size limitations caused by the pump size/capacity of the laboratory-scale 3D-AM system into account. After the CDW-based concrete rubble was crushed in a jaw crusher, it was sieved through a sieve having 2 mm-opening to obtain FCRA and used directly without any treatment to improve the performance. Particle size distribution curve of FRCA is given in Fig. 2.

As alkaline activators, sodium hydroxide solution (NaOH), calcium hydroxide ($Ca(OH)_2$) and sodium silicate (water glass – Na_2SiO_3) were used in different combinations and utilization rates, as will be detailed in following section. NaOH was white, solid and in flake form with purity more than 98%, maximum 0.4% sodium carbonate, 0.1% sodium chloride and a maximum 15 ppm iron. $Ca(OH)_2$ was in powder form with a purity of 87%. Na_2SiO_3 was a sticky, viscous, colorless liquid containing solid material by 55%, with the density of 1.39 gr/cm^3 at 20 °C and SiO_2/Na_2O ratio of 1.9.

2.2. Mixture proportions

A dry base mixture design was devised to efficiently investigate the impact of alkali activator type, concentrations, and combinations on the rheological properties. While 80% the dry base mixture was composed of clay-originated CDW-based precursors (HB, RCB and RT), C and G were both used equally by 10% of the total weight of the base mixture. Considering the fact that the oxide compositions and particle size distributions of HB, RCB and RT were close to each other, they were used in equal amounts, by 26.67% of the total weight of the base mixture (Table 3). C and G were used at limited amounts to support the system of base mixture in terms of CaO and SiO_2, rather than changing the Al_2O_3 balance. The dry base mixture was also incorporated with FRCA, following the aggregate-to-binder ratio of 0.35, which was constant for all mixtures.

In order to optimize the dry base mixture for 3D-AM purposes in terms of rheological properties and compressive strength, NaOH, $Ca(OH)_2$ and Na_2SiO_3 were used solely or in combination for alkaline activation. Three different alkaline activator combinations were used including the single use of NaOH, binary use of NaOH and $Ca(OH)_2$, and ternary use of NaOH, $Ca(OH)_2$ and Na_2SiO_3. Optimum alkaline activator combination and utilization rates were decided based on a systematic study performed step by step. First, the single use of NaOH as the sole alkaline activator was tried, followed by the binary use of NaOH and $Ca(OH)_2$. For these mixtures without Na_2SiO_3, NaOH with molarities of 7.5, 10, 12.5 and 15 M and $Ca(OH)_2$ with utilization rates of 0, 4, 8 and 12%, by the total weight of binder were used crosswise to activate the previously-decided CDW-based dry base mixture. By combining NaOH with $Ca(OH)_2$, it was aimed to benefit from the advantages provided by the calcium addition in the geopolymer system such as fast stiffening,

Table 3
Proportions of geopolymer mortar mixtures.

Alkali activators						CDW-based precursors (g) (1000 g)					FRCA (g)	Si/Al	Na/Si	Ca/Si
NaOH Molarity (M)	Amount (g)	$Ca(OH)_2$ Rate (%)	Amount (g)	Na_2SiO_3 /NaOH	Na_2SiO_3 (g)	HB	RCB	RT	G	C				
7.5	99	0	0	–	–	266.7	266.7	266.7	100	100	350	5.66	0.17	0.30
		4	40									5.66	0.17	0.35
		8	80									5.66	0.17	0.40
		12	120									5.66	0.17	0.45
10	132	0	0	–	–							5.66	0.21	0.30
		4	40									5.66	0.21	0.35
		8	80									5.66	0.21	0.40
		12	120									5.66	0.21	0.45
12.5	165	0	0	–	–							5.66	0.24	0.30
		4	40									5.66	0.24	0.35
		8	80									5.66	0.24	0.40
		12	120									5.66	0.24	0.45
15	198	0	0	–	–							5.66	0.28	0.30
		4	40									5.66	0.28	0.35
		8	80									5.66	0.28	0.40
		12	120									5.66	0.28	0.45
10	132	4	40	1	132							6.04	0.22	0.33
		8	80		132							6.04	0.22	0.38
12.5	165	4	40	1	165							6.14	0.26	0.33
		8	80		165							6.14	0.26	0.38
15	198	4	40	1	198							6.23	0.30	0.32
		8	80		198							6.23	0.30	0.37

initiation of polymerization without high-temperature curing, and improving the compressive strength of the matrix with the formation of further Ca-based gel structure [43]. Na_2SiO_3 was incorporated into some of the developed geopolymer mortar mixtures activated by the binary use of NaOH and $Ca(OH)_2$ (the ones with 10 M-, 12.5 M-, 15 M−NaOH and 4%-, 8%-$Ca(OH)_2$) and the utilization ratio of Na_2SiO_3 was decided based on the constant Na_2SiO_3/NaOH mass ratio of 1 for all mixtures prepared by the ternary blend of NaOH, $Ca(OH)_2$ and Na_2SiO_3. The water-to-binder ratio (w/b) was also constant for all mixtures at 0.33. No chemical admixtures were used during the preparation of the mixtures to prevent any interactions with the alkaline activators, which might endanger the geopolymerization. Proportions of the CDW-based geopolymer mortar mixtures manufactured in the study are shown in Table 3 in detail.

2.3. Mixture preparation and curing

Preparation of geopolymer mortar mixtures started with the preperation of alkaline activators. First, NaOH solutions were prepared at desired molarities by thoroughly dissolving the identified amounts of solid flakes of NaOH within the tap water. Due to high levels of heat release taking place after the exothermic reactions between NaOH solutions were allowed to cool down to ambient temperature before use. Powdery $Ca(OH)_2$ and liquid-form Na_2SiO_3 were directly incorporated into the mixtures.

A mortar mixer was used to mix all the ingredients homogenously. The mixing procedure included the the following steps: (i) first, all the solid ingredients (precursors, FRCA, and $Ca(OH)_2$ (if available for a given mixture) were dry mixed for 60 s at low speed, (ii) NaOH solution was then slowly added to the mixer and all the ingredients were mixed together in the presence of NaOH solution for 60 s at low speed, (iii) Na_2SiO_3 was added to the mixtures (step (iii) was only followed the Na_2SiO_3-containing mixtures), (iv) all ingredients were continued to be mixed for 90 s at low speed and (v) resulting mixture was mixed at a medium speed for additional 60 s and the mixing process was completed.

After the completion of mixing, cubic specimens measuring 50 mm were prepared after casting fresh mixtures into pre-oiled molds. These cubic specimens were first kept in their molds with their surfaces covered with plastic sheets for 24 h at 23 ± 2 °C and 50 ± 5% relative humidity. After the initial 24 h, the cubic specimens were ambient-cured under laboratory environment set at 23 ± 2 °C and 50 ± 5% relative humidity until the predetermined complete testing ages of 7 and 28 days. The remaining portion of the fresh mixtures was utilized for the determination of rheological properties.

2.4. Testing methods

The testing methods used throughout the current work mainly focused on the evaluation of rheological properties and compressive strength of CDW-based geopolymer mortars with the ultimate characteristics fitted for 3D-printability. Rheological property characterization was made by using the fresh-state mixtures via flow table, buildability and vane shear tests. Compressive strength test was used to have an idea about the mechanical properties of the mixtures. Following sections were devoted to details related to the abovementioned test methods.

2.4.1. Flow table test

This test was used for investigation of rheological behavior of CDW-based mixtures against mechanical agitation triggered by the dynamic responses of flow table to simulate both concrete pump and 3D printer, to observe the performance of the mixtures more clearly. Simple empirical method performed by Kazemian et al. [44] and Kim et al. [45] for 3D-printable mixtures was used. The test was performed in accordance with ASTM C1437-15 standard by using a truncated mold. First, the fresh mixtures were filled into the truncated mold placed on the flow table in two layers and each layer was tamped 20 times with the help of a tamper. Then, the mold was removed slowly and flow table was dropped 25 times in 15 s. The diameters in two perpendicular directions were measured after dropping to determine the flowability of the mixtures (Fig. 4). By using the spread values measured after the test, flowability index (Γ) values, as defined by Kim et al. [45], were calculated for each mortar mixture by using the following:.

$$\Gamma = \frac{d_1 d_2 - d_0^2}{d_0^2}$$

where, d_0 is the internal diameter of the mold (100 mm), d_1 is the maximum flow diameter and d_2 is the diameter perpendicular to d_1. Tests were firstly performed on the fresh mortar mixtures immediately after mixing and repeated after 30, 60 and 120 min from the initial mixing to evaluate the rheological changes of the mixtures over time.

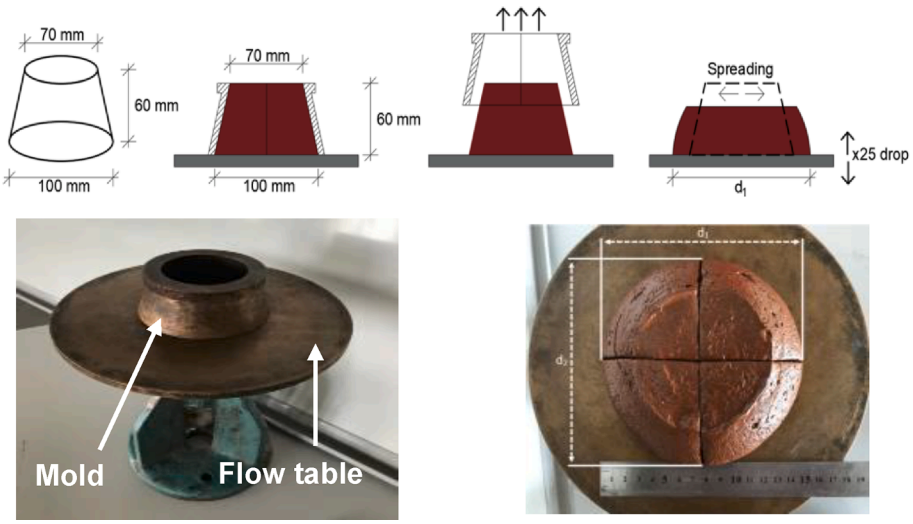

Fig. 4. Schematic drawing (top) and representative images (bottom) showing the details of the flow table test.

2.4.2. Buildability test

Buildability test, a modification of the "mini-slump test" specified in ASTM C1437 standard, was recommended by Nematollahi et al. [23] and used herein to determine the buildability performance (shape retention of the mixtures under static load) of the CDW-based mortar mixtures. Each fresh mixture was placed in the mini-slump mold (the same truncated mold used in the flowability test) shortly after the initial mixing and the mold was slowly removed after 1 min of resting period. Then, a glass plate was placed on top of the fresh specimen to ensure homogeneous distribution of the loading. A 600 g static load (including the weight of the glass plate) was applied to the fresh specimen for 1 min (Fig. 5). At the end of 1 min, the deformation of fresh mixtures was measured in two perpendicular directions by considering the final height of the sample, and the average height was recorded. Mixtures having lower vertical deformation (slump) or higher final height were considered to have better buildability.

2.4.3. Vane shear test

Vane shear test is a simple and effective method to measure flow characteristics of mixtures at fresh state [46,47]. It was used in this study to assess the initial rheological properties of mortar mixtures at fresh state, as well as their open-time performance. Considering the variability of specific yield stress values due to the type and dimensional features of the pocket-type vane shear tool (Fig. 6), the test was used for the comparison of shear yield stress values of geopolymer mortars. Time-dependent results can be also associated with the setting time of the mixtures. For this test, pocket-type vane shear apparatus (with the shear stress capacity of 0–10 N/cm^2 and vane diameter of 48 mm) was used for determining the resistance of mixtures against shear stress.

For the test, firstly, the vane shear apparatus was fully immersed upright into the fresh mortar mixtures. After that, the hand knob located at the top of the apparatus was turned clockwise gradually until achieving the free rotation of the vane and then released. Thereafter, shear yield stress applied by the fresh mixture to the vanes was read from the graduated scale of the apparatus and noted. This test was applied to the mixtures immediately after the completion of mixing (time zero) and repeated after 30, 60 and 120 min from the mixing to monitor the changes in the rheological properties of mixtures over time (open-time).

2.4.4. Compressive strength

Compressive strength tests were performed by using a hydraulic testing machine with 150-ton capacity at a loading rate of 0.9 kN/s in accordance with the ASTM C109 standard [48]. Six ambient-cured cubic specimens with 50 mm dimensions were tested at the curing ages of 7 and 28 days, and the results were averaged.

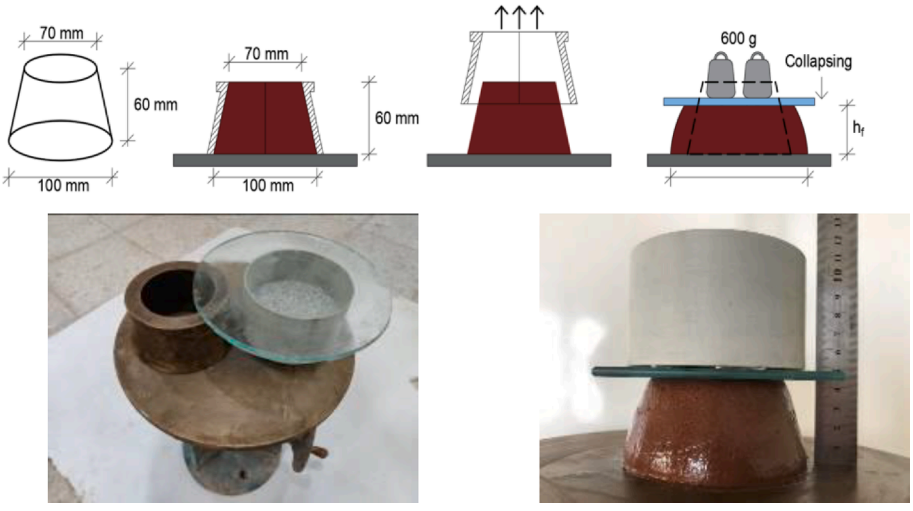

Fig. 5. Schematic drawing (top) and representative images (bottom) showing the details of the buildability test.

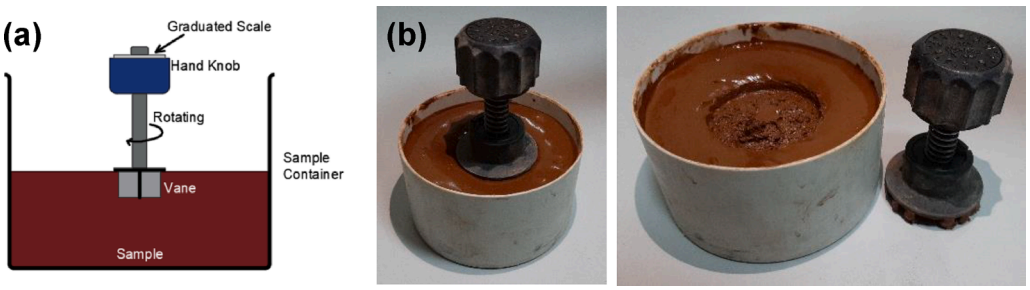

Fig. 6. Schematic drawing (a) and representative images (b) showing the details of the vane shear test.

3. Results and discussion

3.1. Effect of NaOH on the rheological properties

The results of the empirical tests performed to determine the rheological properties of geopolymer mortars and trends obtained due to varying NaOH molarities were presented in Fig. 7. For an easier comparison and clarity, the left-side y-axis of the figure was designed to include both vane shear stress and flowability index, although these parameters were denoted by different legends. An overview of the results indicates that there is a turning point for all the rheological properties tested with the increases in NaOH molarity. The flowability index, which was in an upward trend, and the buildability and vane shear stress results, which were in a downward trend, displayed opposite trends after a certain turning point, where the NaOH molarity was 10 M (Fig. 7).

For further discussion on the observed behavior, the reaction order and integrity of the geopolymerization mechanism, which directly affect the rheological parameters, should be considered. Basically, geopolymerization is a set of reactions consisting of the dissolution of precursors into aluminum and silicon species and polycondensation of aluminosilicate monomers in alkali-activated aqueous solution [49]. Throughout this reaction mechanism, the OH^- ions provided by the alkali hydroxide initiate the process of breaking down the structural bonds of silicon and aluminum available in the precursors, while Na^+, Ca^{2+} and similar positively charged alkali metal ions are responsible for neutralizing the anionic components that dissociate from the precursors [50]. The ion balance of the suspension and the interaction potential (zeta potential) of the precursors are directly affected by the alkalinity and ion concentration of the alkaline activator, which can also affect the formation of geopolymerization products in the medium [51]. Therefore, the properties of alkaline activators and viscosity/ion content of suspension have a vital role on the rheological properties of geopolymers [51]. Increment in the flowability index with an increase in the NaOH concentration up to certain level (10 M−NaOH) was an expected outcome considering the higher dissolution rates of the precursors at higher alkalinity [52,53]. The inclined trend in the flowability index may also be attributed to the non-balanced surface charge of the precursors by Na^+ ions, which can lead to the generation of more repulsive forces and lower yield stress [51]. From this perspective, it can be stated that 7.5 M−NaOH led to lower flowability results due to its limited efficiency of dissolution of the precursors compared to other concentrations. Although further increments in the NaOH molarity were expected to increase the flowability results in line with the abovementioned statements, the trend reversed after 10 M. As stated, while the dissolution rate of the precursor was one of the influential factors for the increased flowability obtained at a certain NaOH molarity (10 M), the presence of non-balanced surface charges in the precursor also seems to be one of the influential factors on the flowability results. Considering the balance of the surface charges of precursors, due to increased Na^+ concentrations in the matrix with the increased NaOH molarity, after 10 M, the surface of precursors is charged with more positive charges, repulsive forces induced by the negative charges on the surface of precursors decreased; thus, geopolymer matrices exhibited higher yield stress [51]. Evident increments took place in the viscosity of NaOH solution after 10 M, which led to higher yield stress for the geopolymer suspension, can be related to decreased flowability results as well [54,55]. With the increased molarity, the amount of ionic species also increases significantly limiting the mobility of ions, which may be another reason for the lower flowability results beyond 10 M−NaOH [52,56]. The geopolymer mortar mixtures produced here incorporated large share of clay-originated CDW-based precursors (Table 3), and the layered structure of clayey precursors is also likely to lead to a reduction in the flowability after 10 M−NaOH due to inter-particle friction causing increased viscosity and stickiness [57].

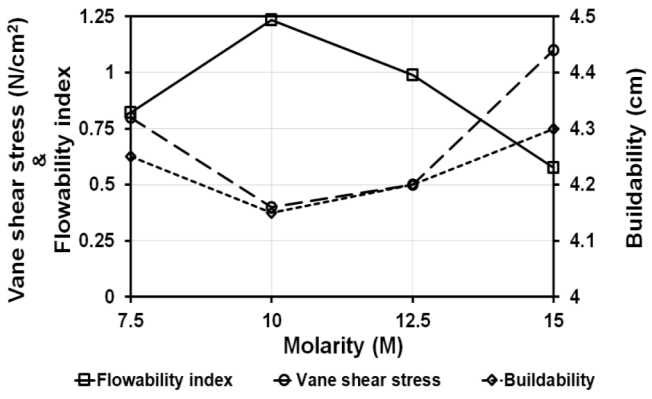

Fig. 7. Changes in the vane shear stress, flowability index and buildability of geopolymer mortars activated by the single use of NaOH solution at different molarities.

Buildability results of the mixtures decreased up to turning point (10 M−NaOH) and then increased (Fig. 7). The decrement in buildability from 7.5 to 10 M was related to increased flowability and decreased yield stress, possible causes of which were discussed above. After 10 M−NaOH, buildability of the mixtures increased was observed. This was most probably due to the acceleration of dissolution of precursors and condensation reactions leading to enhanced geopolymerization and proper stiffening of the matrix through the formation of reaction products contributing to the rigidity and load bearing capacity of the mortars [58]. At different NaOH molarities, vane shear stress results followed a similar trend to buildability results (Fig. 7), therefore explanations for the trend observed for buildability results can be considered valid for the vane shear stress results as well. Although these empirical test methods are considered to be basic and less sensitive to have an understanding on the exact rheological response of the materials, they are clearly useful in acquiring a collective result for the straightforward determination of rheological competencies of such materials for real-time 3D-AM operations.

Time-dependent flowability index and vane shear stress results of the mixtures were given in Fig. 8. Flowability index results of the mixtures were in a decreasing trend, while vane shear stress results were in an increasing trend with respect to time. Similar to the time zero

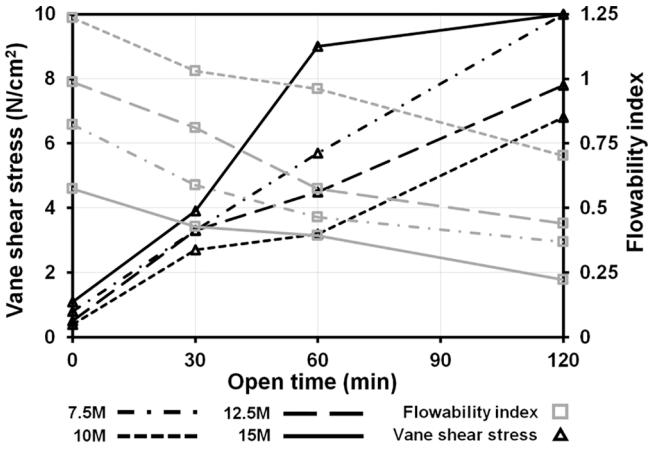

Fig 8. Time-dependent changes in the vane shear stress and flowability index of geopolymer mortars activated by the single use of NaOH solution at different molarities.

measurement, after the end of 30, 60 and 120 min, the highest flowability index value was obtained at 10 M−NaOH, with the decreasing order at 12.5 M-, 7.5 M-, and 15 M−NaOH. The consistency of the vane shear stress tests performed at time zero and after different open times was also valid. The observed time-dependent trend in both flowability index and vane shear stress results was anticipated as the polycondensation phase and aluminosilicate gel precipitation progressed with time [59]. The inverse relationship between the vane shear stress and flowability index results held true for all the time intervals.

After 120 min, the highest decrease in the flowability index results was obtained at 15 M−NaOH while the lowest decrease was observed at 10 M−NaOH, compared to the results obtained immediately after the mixing (time zero). Considering that the increase in the NaOH molarity leads to acceleration in the polymerization reactions [60,61], the dramatic decrement was an expected finding for the mixtures activated by 15 M−NaOH. The mixtures were capable of flowing under relatively low shear forces at the end of 60 min; moreover, even the mixtures that exhibited the highest vane shear values at the end of 120 min still had the capability to flow. Considering this, it may be stated that 3D-AM operations via the hydraulic pressure applied by the concrete pump can be maintained on the CDW-based geopolymer mortars at least 120 min, although different parameters (*e.g.*, hydraulic pressure of the concrete pump) need to be taken into consideration, which are out of scope of current work.

3.2. *Effect of $Ca(OH)_2$ on the rheological properties*

Buildability and flowability index results of geopolymer mortar mixtures activated by the varying molarities of NaOH solution (7.5–15 M) and utilization rates of $Ca(OH)_2$ (0–12%) were presented in Fig. 9 to demonstrate the effects of $Ca(OH)_2$ on the fresh properties of geopolymer mortars. Open-time performances of the geopolymer mixtures were shown in Fig. 10 with respect to vane shear stress and flowability results at time zero and 30, 60 and 120 min after the initial mixing to analyze the time-dependent changes in the rheological properties. Dissolution and condensation start to take place on the surface of precursors upon contact between the alkaline activator and precursor [62,63]. Therefore, the type, rate, combination and distribution of the activators in the medium are effective on the rheological properties of geopolymer mixtures even at the first contact between the precursor and activator during initial mixing.

According to the obtained results shown in Fig. 9, decrements in the flowability index results were observed with the increments in the $Ca(OH)_2$ utilization ratio in the mixtures regardless of the NaOH molarity. Such decrements can be attributed to the effects of $Ca(OH)_2$ on the

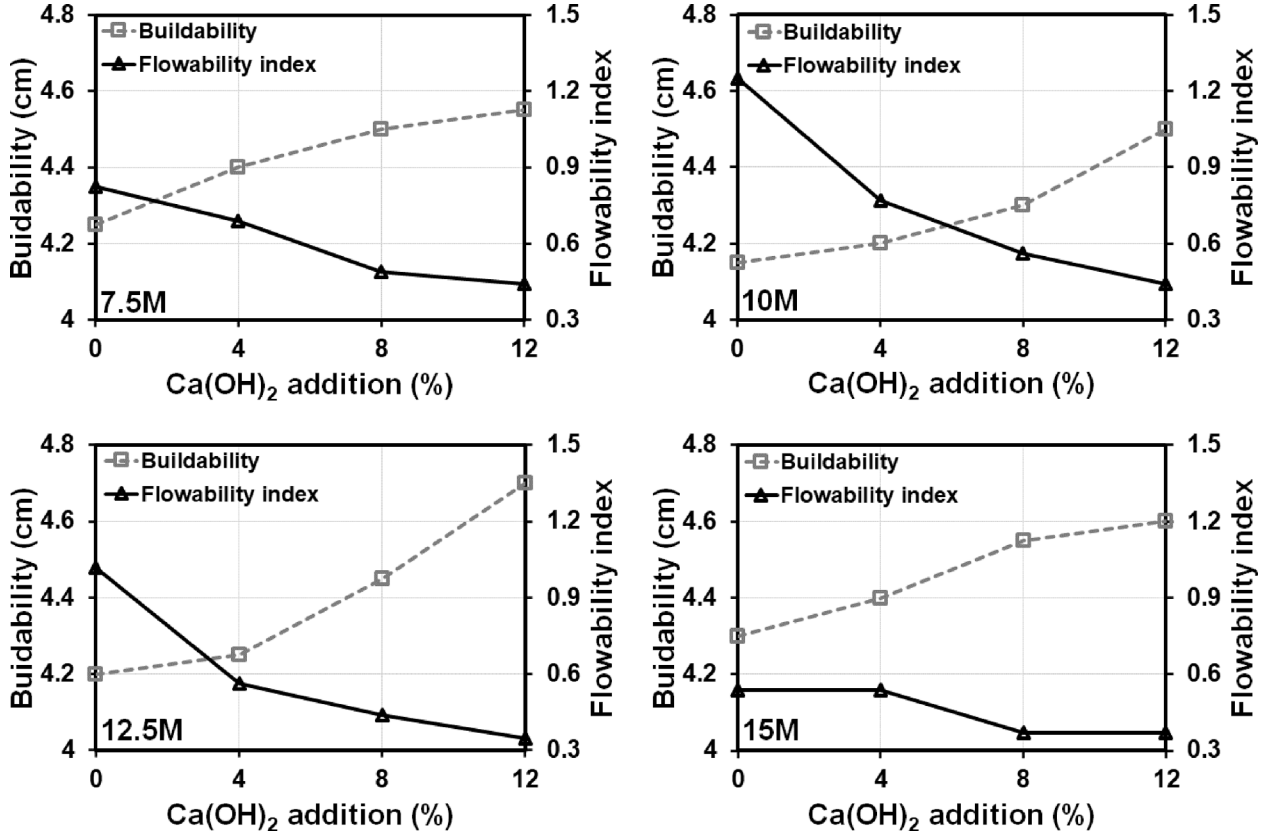

Fig. 9. Buildability and flowability index results of geopolymer mortars activated by the binary use of NaOH and $Ca(OH)_2$.

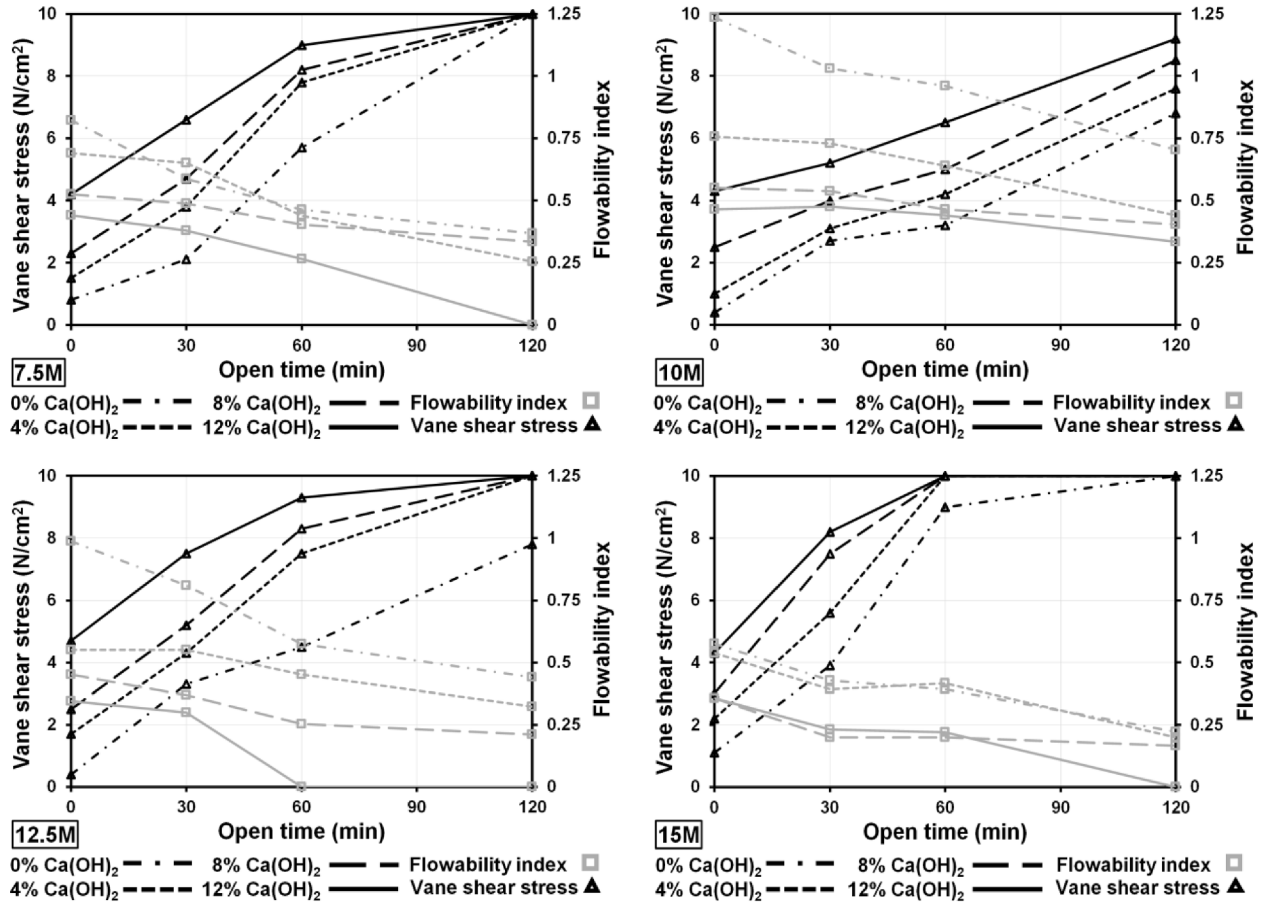

Fig. 10. Time-dependent changes in the vane shear stress and flowability index of geopolymer mortars activated by the binary use of NaOH and $Ca(OH)_2$.

geopolymerization reactions and microstructure of the matrix. Presence of extra OH^- ions in the presence of $Ca(OH)_2$ can promote/enhance dissolution of aluminosilicate precursors, hence lead to the formation of more active groups that will react with the dissolved ions to produce rigidity-improving products [62,64]. However, a balance needs to be ensured regarding the concentration of OH^- ions since higher ionic concentration causes lower ionic mobility on the one hand, but accelerates the condensation thanks to higher amount of dissolved species available in the medium on the other hand [56,65]. Another possible reason for the observed decrement in the flowability can be related to the reactions between increased amounts of $Ca(OH)_2$ available in the medium which reacts with the dissolved aluminate/silicate species and precipitates C-S-H and C-A-S-H gels providing rigidity, and extra nucleation areas for the further formation of geopolymerization products [6,62,65–68]. Furthermore, during the formation of C-S-H and C-A-S-H gels, H_2O molecules in the medium are consumed locally, which results in an increment in the pH as a result of the increased concentration of OH^- ions triggered by condensation reactions (as opposed to dilution effect) and consequently leads to further dissolution of the precursors and formation of geopolymerization [65,67,69]. Moreover, enhanced/faster dissolution of precursors can be attributed to the formation of less protective layers of geopolymer gel on the precursor particles because of the existence of less Si ions and lowered Si/Al ratio available in the medium as a result of the reactions between the Ca and Si ions. Calcium therefore yields better dissolution of particles by preventing the formation of protective layer on the precursor particles, that inhibits further dissolution [66]. Addition of $Ca(OH)_2$ can cause increment in the surface cohesiveness, which can reduce the flowability of the mixtures as well [65]. Increased availability of Ca^{2+} ions with the addition of $Ca(OH)_2$ can also lead to a stronger electrostatic attraction and charge neutralization (charge-balancing) acting as network/ion modifiers that propagate geopolymerization and decrease mixtures' flowability [65,70–72]. Up to 12.5 M−NaOH, changes in the flowability results with respect to the increased $Ca(OH)_2$ utilization rates were clearer. However, for 15 M−NaOH, the effect of increased $Ca(OH)_2$ utilization on the flowability was not as apparent as in lower NaOH molarities (Fig. 9). This can be due to the limitations in the mobility of the ions, which result in slower geopolymerization because of the existence of negatively charged ions as mentioned previously [52,56]. Increments in the buildability results were observed with the increased $Ca(OH)_2$ utilization rates, irrespective of the molarity of NaOH solution (Fig. 9). Such increments in the buildability results with the increased $Ca(OH)_2$ utilization rates were expected and found attributable to the possible reasons affecting the flowability results as discussed above. Vane shear stress results of CDW-based geopolymer mixtures at the initial fresh state increased with the increments in $Ca(OH)_2$ utilization rates, regardless of the molarity of NaOH solution (Fig. 10). This outcome was expected taking the effects of $Ca(OH)_2$ on the microstructural development of geopolymer mortars as discussed above. Moreover, the increments in the vane shear stress results can be explained in a way that $Ca(OH)_2$ addition is favorable for the formation of additional geopolymeric gel products, which create attractive bridging forces increasing the yield stress and viscosity of the system [73].

Vane shear stress and flowability index results were also recorded 30, 60 and 120 min after the completion of initial mixing to observe the time-dependent changes in the mixtures' rheological behavior, which has undeniable effect on the 3D-AM application considering the necessity of maintaining adequate fluidity throughout the printing process. For each mixture, vane shear stress results increased, which was realized

via recording continuously increasing counterforce against the motion of the blades of vane shear apparatus, and flowability index decreased with the extended periods of time due to ongoing geopolymerization reactions. The availability of $Ca(OH)_2$ in the reaction medium with the dissolved CO_3 or CO_2 has been reported to lead to the formation of $CaCO_3$, which can be another reason for the increments in the shear stress and viscosity during different resting periods in addition to the ongoing geopolymerization [64,74]. Although, $Ca(OH)_2$ addition into geopolymers with main-stream precursors was found to have acceleration effect on the setting time of the mixtures [6,65,67], the influence of $Ca(OH)_2$ on the open-time performance of CDW-based geopolymer mortar mixtures was not obvious according to vane shear and flow table test results. The reason for not observing the fast setting in the presence $Ca(OH)_2$ can be attributed to low Si content available in the CDW-based precursors used compared to conventional mainstream precursors (*e.g.*, metakaolin). At the initial phase, dissolved Ca^{2+} tends to react with Si in the medium to form strength-improving products. However, during geopolymerization, available dissolved Si ions in the medium can be limited/diminished, thereby effects of $Ca(OH)_2$ on the setting time may be inhibited as dissolved Ca^{+2} ions may not be capable of reacting with the dissolved Si ions with the extended periods of time.

While determining open-time performance of the mixture, it was considered a time where the capability of vane shear apparatus (10 N/cm^2) and flow table test was exceeded. Entirely CDW-based geopolymer mortar mixtures activated by the binary combination of NaOH and $Ca(OH)_2$ showed an open-time performance ranging from 60 to 120 min, except the mixtures activated by 10 M−NaOH. Although the vane shear apparatus was incapable of measuring the consistency of some mixtures activated by 7.5 M-, 12.5 M-, and 15 M−NaOH after longer resting periods (60–120 min), flow table test results showed that the mixtures were still in fresh-state after the given resting periods and flowed under dynamic load, although slightly. Vane shear stress results equal to or greater than 10 N/cm^2 (beyond the capacity of apparatus) do not mean that the mixtures have completely lost their workability and hardened. Such discrepancies in the results can be attributed to the differences in the testing methods. Overall, the mixtures activated by 10 M−NaOH at all $Ca(OH)_2$ utilization rates had longer open-time periods (even 120 min after the initial mixing), although they were workable and capable of being tested via flow table and vane shear apparatus.

3.3. *Effect of Na_2SiO_3 on the rheological properties*

Taking the test results obtained from mixtures prepared by the binary use of NaOH and $Ca(OH)_2$ into account, Na_2SiO_3 was finally incorporated into the geopolymer mortar mixtures to modify/upgrade the properties, especially at the hardened state, considering that the incorporation of Na_2SiO_3 would provide extra reactive Si ions in the reaction medium. Since considerably faster hardening response was obtained in the trials performed at Na_2SiO_3/NaOH mass ratios higher than 1, Na_2SiO_3/NaOH mass ratio was chosen 1 for all the mixtures prepared by the ternary use of NaOH, $Ca(OH)_2$ and Na_2SiO_3. In mixtures with the ternary blends of activators, $Ca(OH)_2$ utilization ratio was chosen to be either 4 or 8% of the total weight of the binder as these rates have resulted in higher strength and more stable consistency for the mixtures with the binary blends of NaOH and $Ca(OH)_2$. For NaOH, molarities of 10, 12.5 and 15 M were chosen considering the effects of Na/Si ratio on the geopolymerization mechanism. Flow table and vane shear tests (0, 30, 60, 120 min after the completion of initial mixing) and buildability test were performed on the produced mixtures. Flow table, vane shear and buildability test results of the geopolymer mortars performed shortly after the preparation of the mixtures were illustrated in Fig. 11. Test results of mixtures activated by the binary (NaOH + Ca

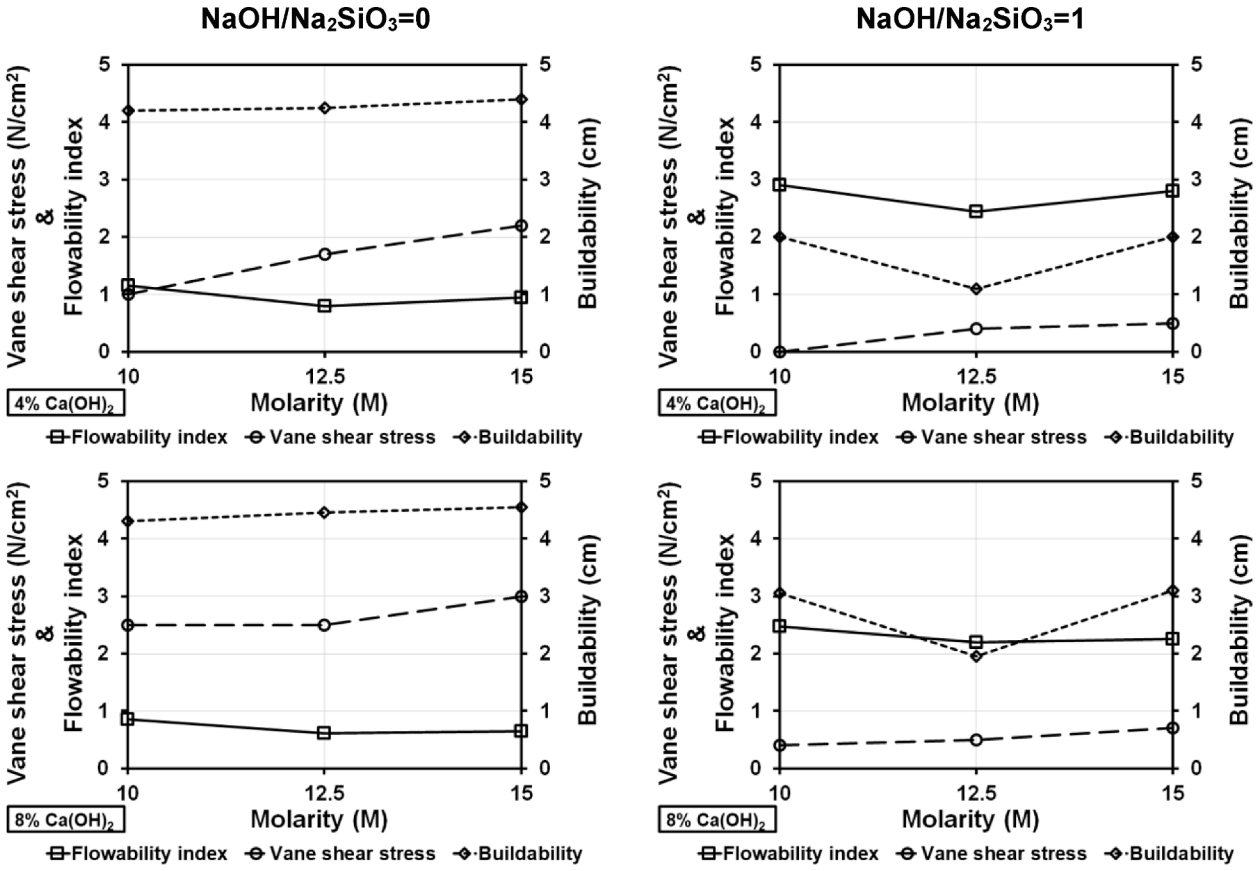

Fig. 11. Vane shear stress, flowability index and buildability results of geopolymer mortars activated by the binary use of NaOH and $Ca(OH)_2$ on the left or ternary use of NaOH, $Ca(OH)_2$ and Na_2SiO_3 on the right.

$(OH)_2$) and ternary ($NaOH + Ca(OH)_2 + Na_2SiO_3$) use of activators were shown together in Fig. 11 for an easier comparison of the fresh properties and better display of the effect of Na_2SiO_3 on these properties.

When the flowability results were evaluated, it was observed that the addition of Na_2SiO_3 into the geopolymer mortar mixtures made a significant contribution to the initial flowability at the fresh state (Fig. 11). When other variant mixture parameters (*e.g.*, NaOH molarity and Ca $(OH)_2$ utilization rates) were the same, although it is a high-viscosity fluid, incorporation of Na_2SiO_3 solution, irrespective of the mixture configuration, caused significant reductions in the viscosity of the mortar mixtures, thereby higher spreading levels under the effect of agitation induced by the flow table test. Higher flowability of the Na_2SiO_3-containing mortar mixtures can be attributed to plasticizing and deflocculating (dispersing) effect of the alkali silicate solutions due to the absorption of silicate species on the precursor powder surfaces, which results in negative surface charging of the powders, and thereby interparticle repulsive forces between the similarly charged particles [51,75–79]. Although the initial flowability of the Na_2SiO_3-containing geopolymer mortars was high, according to the results of flow table tests performed after different resting periods of 30, 60 and 120 min starting from the completion of initial mixing, it was found that the mixtures hardened rapidly by losing their fluidity/consistency in less than 30 min, regardless of the different mixture design parameters. This was a likely outcome and attributed to the increased amounts of reactive soluble silica coming from Na_2SiO_3, resulting in an enhancement/acceleration in the geopolymerization reactions/gel formation (*e.g.*, C-S-H) and faster water loss, thereby faster hardening and shorter open-time period compared to mortar mixtures without Na_2SiO_3 [72,76,80–83]. It is also possible to mention as one of the reasons of rapid hardening response of the Na_2SiO_3-contaning mixtures that the incorporation of $Ca(OH)_2$ as an additional Ca^{2+} source in these mixtures provided more wide-spread availability of the Ca^{2+} ions in the medium to react with $[SiO_4]^{4-}$ from Na_2SiO_3, and thereby led quick "primary C-S-H" formation causing hardening [84]. Considering the fact that one of the main requirements expected from 3D-printable mixtures is sufficient open-time period, which necessitates maintaining acceptable flowability for the pumping/extrusion of the material over a certain period of time, the tendency of Na_2SiO_3-containing geopolymer mortars to lose their flowability rapidly (significantly reducing the workable time period of the mortar mixtures) makes these mortar mixtures relatively unsuitable for the 3D-printing purposes, especially for the cases, where high volumes of material and therefore longer production periods are necessary.

Similar to the flowability results, there was a general trend in the vane shear stress and buildability results of mixtures with and without Na_2SiO_3. A decreasing trend of initial viscosity of the geopolymer mortars was observable in the presence of Na_2SiO_3 as evidently inferred from the buildability and vane shear stress results (Fig. 11). After the buildability tests, the average final heights of mortar mixtures with Na_2SiO_3 were measured to be markedly lower than those without, irrespective of other mixture design parameters, which means that the incorporation of Na_2SiO_3 caused easier collapse under static load, thereby reduced capability to remain in position. For the studied mixtures, in terms of 3D-AM applicability, it can be therefore stated that the incorporation of Na_2SiO_3 can cause mixtures not to retain their extruded shapes under self-weight and stresses embarked by the consecutive upper layers. Besides, it was clear that the resistance of the mixtures to the shear force imposed by the vane shear stress test device decreased significantly with the Na_2SiO_3 inclusion as can be followed from Fig. 11. On the other hand, as in flowability results, the vane shear tests performed over different periods of 30, 60 and 120 min after the completion of mixing showed that Na_2SiO_3-included mixtures became stiff in less than 30 min, irrespective of the different mixture compositions. Based on these findings, it can be stated that Na_2SiO_3 inclusion caused rapid hardening of the CDW-based geopolymer mortars and had a lower open-time; therefore negative effects on the extrudability/buildability and transmission of the mixtures through a closed system (*e.g.*, 3D-printing equipment). To conclude, mixtures produced by the use of ternary blends of NaOH, $Ca(OH)_2$ and Na_2SiO_3 as the alkaline activators had higher flowability (lower viscosity) initially compared to those produced by the binary blends of NaOH and $Ca(OH)_2$ although these mixtures exhibited faster setting/hardening and rapid increase in shear resistance over time. Apart from the abovementioned statements, with the changes in the molarity of NaOH and utilization ratio of $Ca(OH)_2$, the rheological behaviors of the mortar mixtures produced by the ternary blends of alkaline activators were found to be similar to mixtures produced by the binary blends of alkaline activators. Since the changes in the rheological properties of different mixtures based on the variations in NaOH molarity and $Ca(OH)_2$ content were discussed previously, no further comments were made here.

3.4. Effect of different alkaline activator combinations on the compressive strength

Average compressive strength test results of 7- and 28-day-old geopolymer mortar mixtures produced by the single use of NaOH, binary use of $NaOH + Ca(OH)_2$ (Fig. 12-a) and ternary use of $NaOH + Ca(OH)_2 + Na_2SiO_3$ (Fig. 12-b) were presented in Fig. 12. For the mixtures activated by NaOH singly, increased NaOH molarities resulted in general increments in the results, irrespective of the age. Strength development was expected given the increments in the amounts of dissolved particles and increased surface area of dissolved particles that were charged by the cationic ions of alkali activators with the increments in NaOH molarity [52,53,60]. For the 28-day-old specimens, excessive increments in the NaOH molarity (15 M) caused no changes or slight decrements in the compressive strength results. This finding can be attributed to the excessive number of ions in the system causing repulsive forces between particles [52,54,56]. As a result of the repulsion-induced restriction on the ionic mobility, heterogeneous regions consisting of non-reacted particles may form, which eventually act like flaws in the microstructure of the matrix.

Incorporation of $Ca(OH)_2$ into NaOH-activated mixtures resulted in compressive strength results to increase, as $Ca(OH)_2$ gets involved in the alkaline activation process and modifies the characteristics of the reaction products. More specifically, such increments can be attributed to the effects of $Ca(OH)_2$ including the enhanced dissolution of the precursors with the higher-alkalinity medium, ionic charge balancing, seeding effect, $CaCO_3$ formation and further formation of strength-improving products, leading to more compact, homogenous, and finer microstructure [6,56,64–66,70–72,74]. Additional products formed in the presence of $Ca(OH)_2$ are likely to fill the voids and pores of the matrix during ambient curing bridging different geopolymerization products, hydrated phases and unreacted precursors, thereby increasing the compressive strength of the mixtures. Although the increased Ca $(OH)_2$ utilization rates within the mixtures activated by higher-molarity (12.5 and 15 M) NaOH, favored the compressive strength development at the end of 28 days of ambient curing, for the mixtures activated by lower-molarity (7.5 M and 10 M) NaOH, the effects of $Ca(OH)_2$ utilization beyond 4% were not considerable. This outcome can be attributed to the excess amounts of lime disrupting the optimal gel binder structure and delaying the formation of additional products as it can disturb the Si/Al ratio locally, which can cause less homogeneous microstructure [65]. Moreover, extra lime may not be involved in the geopolymerization products and may remain unreacted, which leads to the formation of flaws in the microstructure. Such behaviors are more evident at lower NaOH molarities due to the existence of lower available reactive dissolved Si and Al species because of lower dissolution of precursor particles at lower alkalinity [52,53].

In accordance with the results shown in Fig. 12-a, $Ca(OH)_2$ addition was more favorable/influential for the 28-day ambient-cured geopolymer mortars considering 7-day results. Such finding could be attributed to the lowered alkalinity at later age because of ongoing geopolymerization during ambient curing, since C-A-S-H formation with

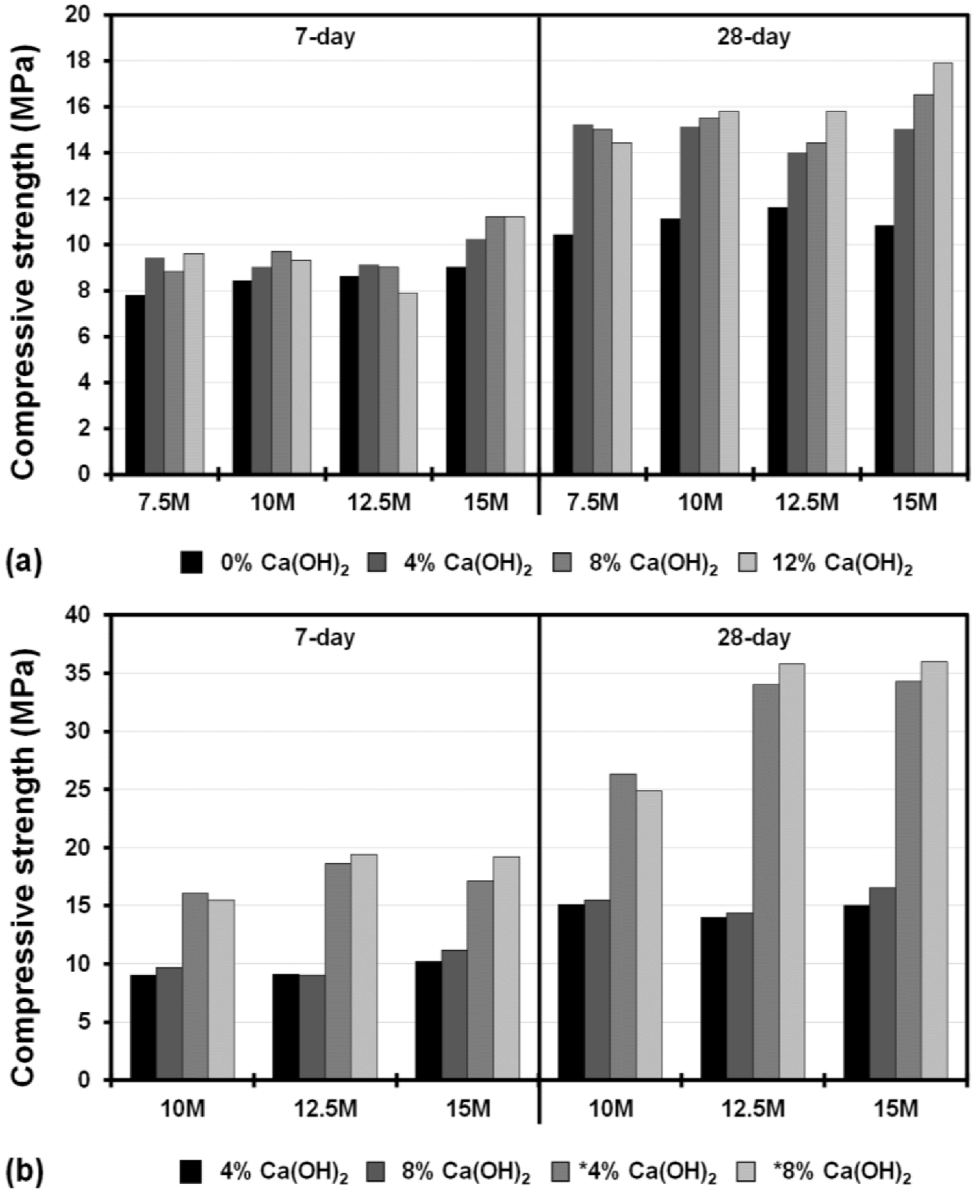

Fig. 12. Average compressive strength results of geopolymer mortars activated by the use of different alkaline activator combinations. (a) Binary use of NaOH + $Ca(OH)_2$, (b) Ternary use of NaOH + $Ca(OH)_2$ + Na_2SiO_3 (*represents the mixtures containing Na_2SiO_3).

the incorporation of $Ca(OH)_2$ is more prevalent at lower alkalinity levels [56]. Overall, the alkalinity is one of the main parameters determining the compressive strength of CDW-based geopolymers. On one hand, the high molarity leads to higher dissolution of the precursor but restricts the effects of $Ca(OH)_2$ on the formation of C-A-S-H at early ages, on the other hand, lower molarity induces the effects of $Ca(OH)_2$ yet decreases the dissolved ions in the reaction medium. At the end of 28 days of ambient curing, entirely CDW-based geopolymer mortars activated by the binary use of NaOH and $Ca(OH)_2$ resulted in a maximum compressive strength of 17.9 MPa.

As it is clear from Fig. 12-b, the incorporation of Na_2SiO_3 into the geopolymer mortar mixtures improved the compressive strength results for all the curing ages and this behavior seemed to be valid for all the mixtures produced by different activator proportions (*i.e.*, different NaOH molarities and $Ca(OH)_2$ utilization rates). Compressive strength development rates of Na_2SiO_3-containing mixtures from 7 to 28 days were also higher than those of non-Na_2SiO_3-containing mixtures. These findings implied in regard to the enhancement of compressive strength results of geopolymer mortar mixtures that the incorporation of Na_2SiO_3 into the binary blend of NaOH + $Ca(OH)_2$ is an effective option. Improvements noted in the compressive strength results of geopolymer mortars in the presence of Na_2SiO_3 can be related to the following: (i) stimulation/acceleration of geopolymerization reactions in the presence of increased amounts of highly soluble reactive silica and reactions [85–87], (ii) stimulation/increase of the production of shorter and stronger Si-O-Si bonds in comparison to Si-O-Al and Al-O-Al bonds due to increments in the SiO_2/Al_2O_3 ratio [88–91], resulting in stronger geopolymer bonds and denser/stiffer microstructure (Si-rich aluminosilicate gel) [92,93], (iii) increase in the pH (therefore dissolution of precursors) and further activation of the reactions [94] and (iv) higher rate of initial C-S-H gel production as a result of the reactions between dissolved Ca^{2+} [83]. The maximum 28-day compressive strength of around 36 MPa was obtained from the mixtures activated by the ternary blends of NaOH, $Ca(OH)_2$ and Na_2SiO_3.

Although relatively high compressive strength results were achieved with the use of Na_2SiO_3, when considering the requirements in terms of fresh state properties, it was clear that non-Na_2SiO_3-containing mixtures were more appropriate for 3D-printing application. Therefore, some of

the non-Na_2SiO_3-containing mixtures were selected to be printed, as detailed below. Although compressive strength results of 28-day ambient-cured CDW-based geopolymer mixtures activated by the single use of NaOH or binary usage of NaOH and $Ca(OH)_2$ can be considered relatively low regarding the conventional geopolymer and concrete used in structural elements, compressive strength values obtained from these mixtures can be regarded as acceptable for non-structural purposes. However, after generating the data base regarding the rheological properties and the parameters affecting the rheology, it is possible that compressive strength development can be improved with several approaches such as increasing fineness of precursor particles, incorporation of additional Al and Si sources and heat curing application, etc. [8,38,95].

3.5. Comparison of rheological properties of CDW-based geopolymer mortars and corresponding paste phases

In order to have an understanding on the effect of the fine recycled concrete aggregates (FRCA) inclusion on the properties of CDW-based geopolymers, test results obtained from mortar mixtures prepared in the current study were compared with the companion CDW-based geopolymer binders (paste) of the recently published study of the authors [38]. The precursor composition of both mortar and paste mixtures were composed of CDW-based materials almost identical to each other. The only difference was that the precursor blend of the mortar mixtures included a minor content of C. CDW-based precursors used in both studies were obtained from the same source and were with identical chemical/physical properties. Table 4 tabulates the rheological property test results of representative rheological test results of the mortar and paste mixtures for comparison. The results of selected mixtures having similar alkaline activator combinations/amounts were shown for an easier comparison.

As can be followed from Table 4, the flowability index values of the mortar mixtures were lower than those of paste mixtures and the buildability results increased when the paste mixtures were incorporated with FRCA, regardless of the selected alkaline activator combination. These results clearly show that FRCA inclusion into geopolymer pastes increases the viscosity/consistency, which can be attributed to the increased solid fraction and interparticle friction [96,97]. When the vane shear stress results of the paste and mortar mixtures were compared, it was seen that the vane shear stress results of the mortar mixtures were lower than those of paste mixtures. This was found contradictory since it was considered that the vane shear stress results would follow a trend similar to flowability index/buildability results and attributed to the nature of pocket-type vane shear stress apparatus. According to the working principle of this apparatus, the operation-/calibration-related parameters are significantly influential on the recorded shear stress results measured and it was reported that variable shear stress results can be obtained depending on the vane of the test apparatus, calibration, test techniques and residual deformation of spring as a result of the repeated use [98]. Although the vane shear stress results of paste and mortar mixtures were in conflict with the generally expected trend, shear stress results of paste and mortar mixtures were consistent within themselves and useful in determining the effect of different types/amount of alkaline activators on the rheological properties of the mixtures. Considering the variations observed in the vane shear stress results of these two different phases, it is therefore suggested to use a newly-calibrated vane shear apparatus by implementing tests under same operational conditions to compare the relative shear stresses of geopolymer mixtures, more precisely. Together with vane shear test, performance of additional tests is also suggested that to account for possible drawbacks of the vane shear apparatus, which is a basic test method.

Although the inclusion of FRCA resulted in increments in the viscosity/consistency of the geopolymer pastes, mortar mixtures with suitable rheological properties for 3D-AM were successfully developed without incorporating any chemical admixtures. In terms of the compressive strength results, there was no adverse effect of adding FCRA into geopolymer pastes since the results were found comparable for both paste and mortar mixtures although it is expected that utilization of FRCA causes reduction in compressive strength performance because of the presence of originally interfacial transition zone (ITZ) between original aggregates and residual paste/mortar particles and additional ITZ forming between the geopolymeric binder and recycled aggregates. This result can be explained in a way of that the old, hardened cement attached to the crushed aggregates may participate in depolymerization as a source of silicon / calcium and result in a good bond between the new binder and old aggregates [99].

Table 4
Rheological property test results of the CDW-based geopolymer pastes and mortars.

NaOH (M)	Ca $(OH)_2$ (%)	Mixture phase	Flowability index	Buildability (cm)	Vane shear stress (N/cm^2)
7.5	0	Paste	1.67	3.60	3.8
		Mortar	0.82	4.25	0.8
	4	Paste	1.45	3.85	4.0
		Mortar	0.69	4.40	1.5
	8	Paste	1.19	3.95	4.5
		Mortar	0.49	4.50	2.3
10	0	Paste	1.83	3.55	3.3
		Mortar	1.25	4.15	1.5
	4	Paste	1.44	3.80	3.3
		Mortar	0.77	4.20	1.0
	8	Paste	1.18	3.95	3.3
		Mortar	0.56	4.30	2.5
12.5	0	Paste	1.86	3.60	3.0
		Mortar	1.02	4.20	2.3
	4	Paste	1.46	3.80	3.6
		Mortar	0.56	4.25	1.7
	8	Paste	1.19	3.95	3.6
		Mortar	0.44	4.45	2.5
15	0	Paste	1.87	3.50	1.6
		Mortar	0.54	4.30	4.2
	4	Paste	1.49	3.80	2.5
		Mortar	0.54	4.40	2.2
	8	Paste	1.27	3.85	3.1
		Mortar	0.37	4.55	3.0

3.6. Laboratory-scale 3D-AM application

The suitability of entirely CDW-based geopolymer mortars to printing process was evaluated by using a laboratory-scale 3D printer, details of which were given in Fig. 13. In order to demonstrate the correlation of empirical testing methods with the ultimate 3D-AM products, and investigate the 3D-printing performance of the mixtures having different rheological properties, two geopolymer mortar mixtures with no additional chemical admixtures other than alkaline activators were printed. For the determination of effects of rheological differences on the ultimate products more precisely, mixtures having high and low viscosities were selected to be printed.

Compressive strength and open-time performances were also taken into consideration during the selection of mixtures. The mixture activated by 10 M−NaOH had lower viscosity and more extended open-time. The effect of $Ca(OH)_2$ utilization ratio after 4% was negligible on the compressive strength of the mixtures at lower NaOH molarities. Thus, the mixture activated by the binary use of 10 M−NaOH and 4%-$Ca(OH)_2$ was chosen to represent the high-workability (low-viscosity) mixture performance (Mixture-A). As the mixture activated by the binary use of 15 M−NaOH and 12%-$Ca(OH)_2$ showed higher viscosity and compressive strength among all mixtures, it was chosen to represent the low-workability (high-viscosity) mixture performance (Mixture-B). In order to analyze the quality of the mixtures regarding the flowability,

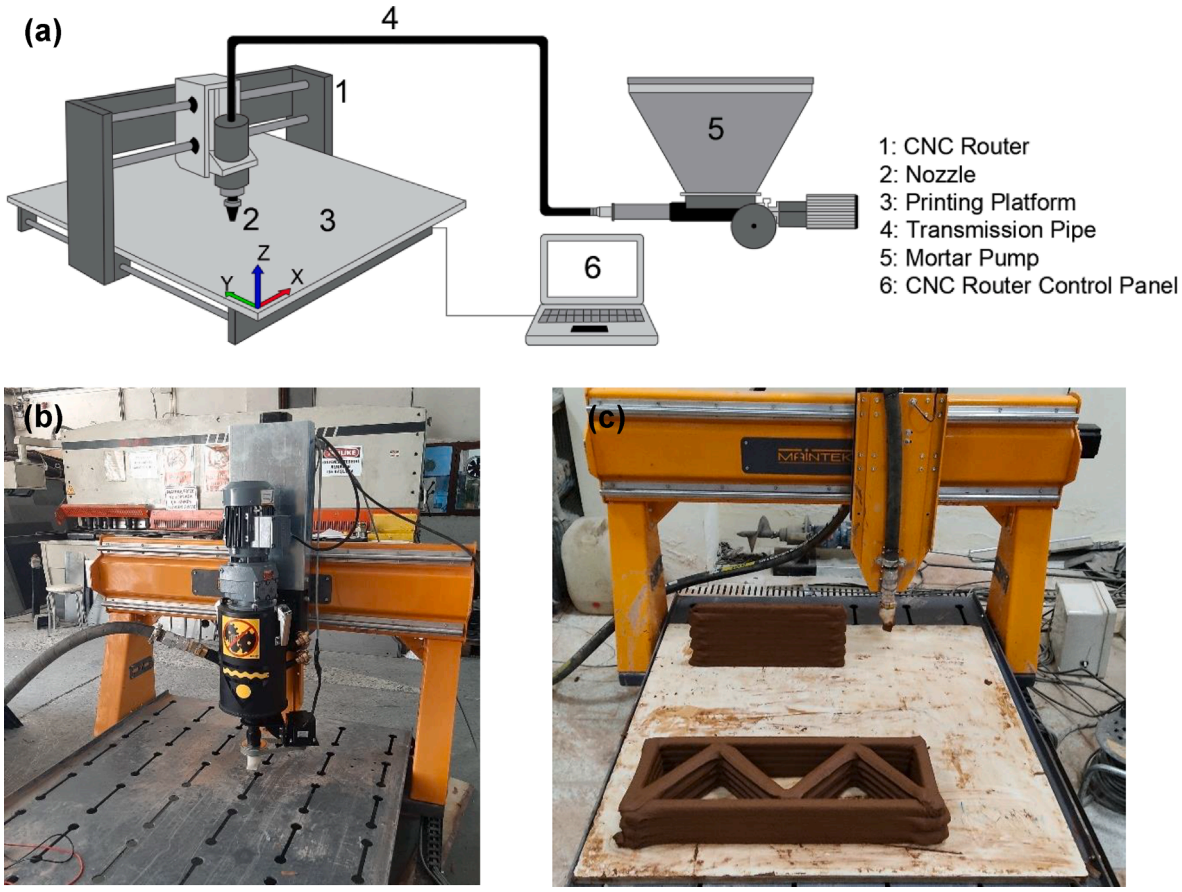

Fig. 13. (a) Detailed parts, (b) real-time view and (c) in-operation image of the laboratory-scale 3D printer.

buildability, continuity and surface quality, the mixtures were printed in a single- and multi-layered way and the printed specimens were investigated via visual inspection by focusing on the cracks/defects/ruptures formed and the dimensions by considering the shape retention ability. For the 3D-printing operation, a nozzle having a 20 × 20 mm cross-section was used and the operational printing speed (the movement speed of the printer-head) was set to 60 mm/s.

At the visual inspection stage, initially single-layer printed specimens of the two selected mixtures were examined to understand whether a continuous/homogeneous layer structure was formed for determining the factors that disrupted the continuity, and analyzing the ability of mixtures to maintain dimensional stability. The determination of the reference/base layer height with a single-layer printed specimen is critical for the high-accuracy evaluation of the buildability performance of the mixtures individually and to eliminate the height differences resulting from level variations of the printing bed. Therefore, the heights of single-layer specimens were measured to determine a reference/base layer height to compare the height changes in multi-layer specimens.

Visual inspections showed that utilization of mixture with the combined use of 10 M−NaOH + 4%-$Ca(OH)_2$ (Mixture-A) had a more continuous flow than the mixture with the combined use of 15 M−NaOH + 12%-$Ca(OH)_2$ (Mixture-B) and had a structure with less defects/voids/fractures (Fig. 14). Such outcomes were expected considering the flowability index values of both mixtures. Due to its higher flowability, Mixture-A exhibited a higher level of consistency/accuracy/adaptability with the designed G-code of the printed specimen on both horizontal (Fig. 14-a) and vertical printing directions (Fig. 14-c, d). However, while Mixture-B had a consistent/suitable layer height in regard to the design code in the vertical direction with its higher buildability value (Fig. 14-c,d), it exhibited insufficient performance in the horizontal direction due to flow discontinuity and stiff structure (Fig. 14). This finding was related to the movement restriction of high viscous Mixture-B from the feeding bunker of the pumping system to the screw pump decomposition mechanism due to its stiffer nature. Along with the material-/printer-related defects, some negligible defects formed on the top surface of the specimens caused by the residues of mortar particles remaining on the nozzle edges.

Images of the multi-layer printed versions of the mixtures were given in Fig. 14-c,d. The multi-layer printed specimens exhibited similar properties to the single-layer printed ones; Mixture-A with higher flowability/lower viscosity had no discontinuity in layers with a negligible number of defects, while Mixture-B with lower flowability/higher viscosity had non-continuous layers with high number of defects. Results of dimensional measurements of the specimens printed as single- and multi-layer were given in Table 5. The heights of the single-layer specimens were considered reference layer height in line with the abovementioned considerations. To evaluate the buildability performances of the multi-layer specimens, the layer heights measured from 10 different points of 20 cm-middle part of each 30-cm layer were averaged, and the height differences (in percentage) compared to the reference layer height were calculated by using the following equation for each layer individually.

$$Height\ difference(\%) = \frac{h_i - h_0}{h_0} \times 100$$

where, h_0 represents single layer height and h_i stands for multi-layer height.

The ultimate buildability performances of multi-layer specimens were calculated by the ratio of the actual final height of the printed structure to the final height determined in G-code (220 mm [20 × 11 mm]: height of the structure with 11 layers) (Table 5). In addition, the

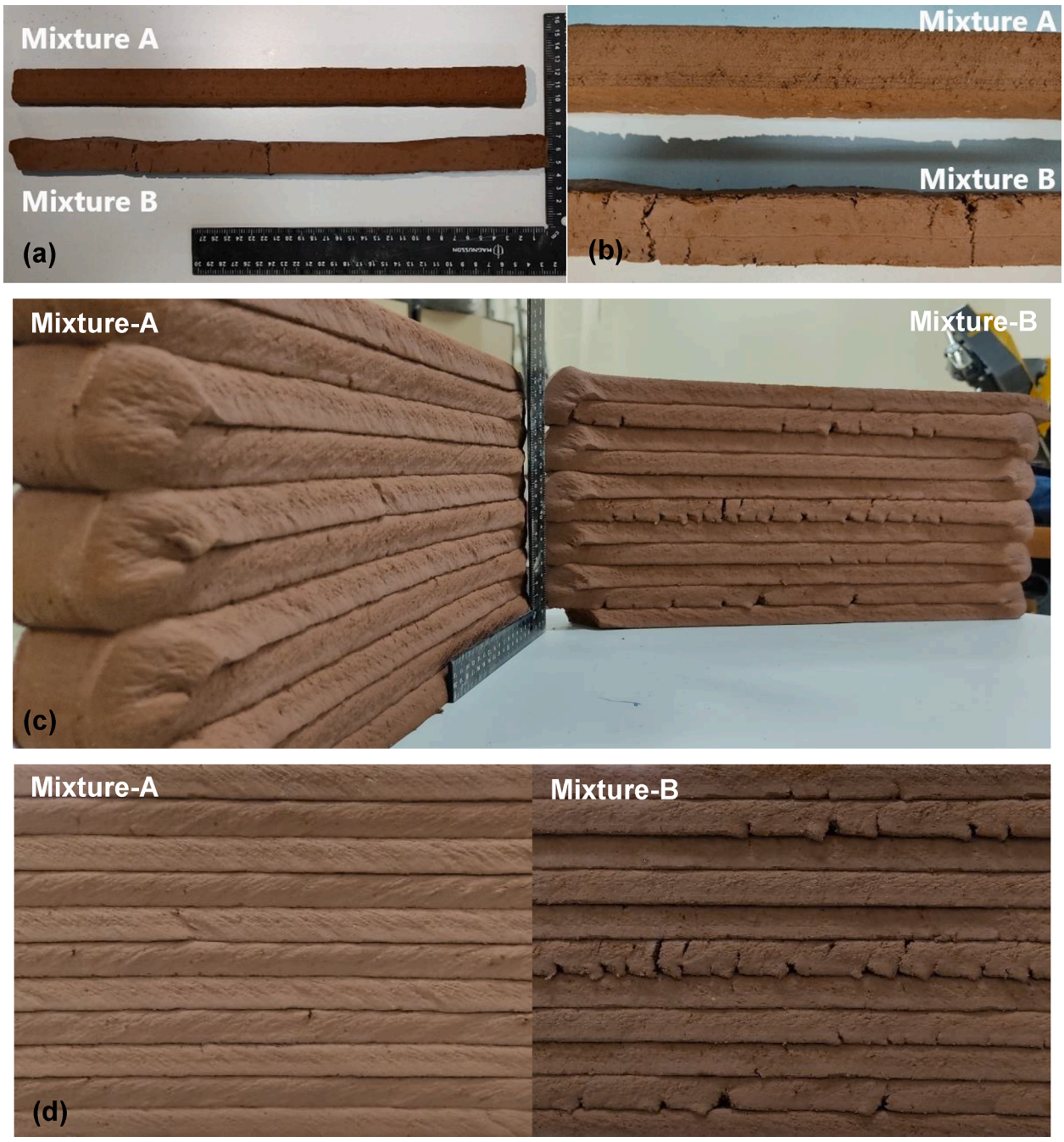

Fig. 14. (a) General, (b) close-up view of single-layer specimens of 3D printed geopolymer mortar mixtures showing the defects and (c) general, (d) close-up views of multi-layer specimens of 3D printed geopolymer mixtures.

ultimate settlement was calculated by taking the difference between the height of the targeted structure determined in G-code (220 mm) and the height of the printed structures (206.95 mm and 213.99 mm for Mixture-A and -B, respectively). As expected, the height of each layer showed variations in relation to the number of layers overlying on each one of them. While the settlement results were high in the lower-level layers of the multi-layer specimens with respect to the height of reference layer, less settlement occurred at upper-level layers due to decrements in the amount of load carried by the consecutive upper layers. Buildability of the multi-layered structures, which was determined by using equation given below.

$$Buildability(\%) = \left(1 - \frac{H_d - H_f}{H_d}\right) \times 100$$

where, H_d and H_f stand for the total height of the virtual structure designed by the 3D printer software and the final total height (collapsed) of real-time printed structure, respectively. Buildability results were recorded as 94.1% and 97.3% for Mixture-A and Mixture-B, respectively. Considering that the buildability results of the mixtures obtained by the empirical test methods are close to the results obtained after real-time 3D-printing (percentage equivalent of 84% for Mixture-A [collapsing from 5 to 4.2 cm] and 92% for Mixture-B [collapsing from 5 to 4.6 cm]), the capability of the empirical test methods in predicting the performance of 3D printed end product is clear.

In Fig. 15, a close-up image of the nozzle taken during the printing operation of Mixture-A was presented. Defects were observed at the lower (bottom) surface of the layer immediately after the material extrusion from the nozzle, which can be associated with the tension

Table 5
Dimensional properties of 3D printed geopolymer mortar mixtures (units are in mm).

# of layers	Mixture-A 10 M NaOH − 4% $Ca(OH)_2$ Single-layer	Mixture-B 15 M NaOH − 12% $Ca(OH)_2$ Multi-layer	Height difference (%)	Single-layer	Multi-layer	Height difference (%)
1	19.85	17.52	−11.74	19.97	18.50	−7.36
2		17.78	−10.43		19.00	−4.86
3		18.25	−8.06		19.21	−3.81
4		18.39	−7.36		19.34	−3.15
5		18.82	−5.19		19.35	−3.10
6		19.02	−4.18		19.55	−2.10
7		19.11	−3.73		19.62	−1.75
8		19.26	−2.97		19.79	−0.90
9		19.48	−1.86		19.78	−0.95
10		19.50	−1.76		19.90	−0.35
11		19.82	−0.15		19.95	−0.10
Total		**206.95**			**213.99**	
Buildability (%)	**94.1**	**97.3**				
Ultimate settlement (mm)	**13.05**	**6.01**				

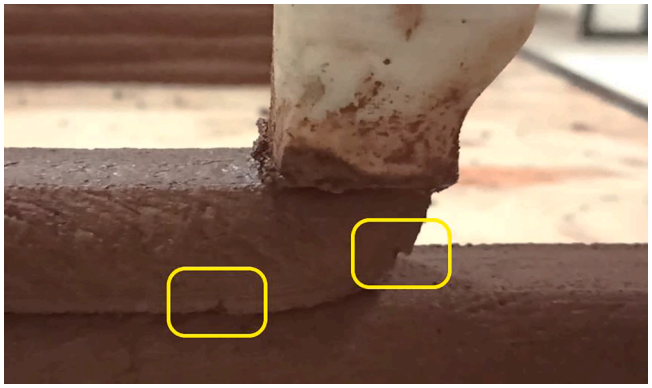

Fig. 15. A close-up image of the nozzle taken during the printing operation of Mixture-A.

forces exerted on the material between the end of the pump and the contact region with the sub-layer. Any fluctuation that may occur during the flow of the material in 3D-AM system may instantly cause a stress concentration between these two regions and result in a defect formation. Another reason for the formation of defects in the printed layer can be associated with the operational compatibility between the 3D printer and the pump. Even though the material has suitable rheological parameters for printability, if the compatibility of the 3D printer and the pump system cannot be ensured precisely, the designed geometries cannot be printed with high-accuracy/-quality, and the ultimate product may have defects.

In Fig. 16, different images taken during the printing operation of Mixture-A were presented, and a defect that occurred on the printed layer was highlighted. As can be followed from Fig. 16-a to c, the defect that occurred gradually expanded with the tensile forces created as a result of the movement of the nozzle in the printing direction. This can be attributed to the discordance of the printing speed of the 3D printer and the material transfer speed of the pump for a certain period of time, or the discontinuities and/or air gaps that occurred when the material feeds the pump.

A pre-designed structure was printed by using Mixture-A in the laboratory-scale 3D printer to demonstrate the shape retention ability, buildability performance, and relationship/compatibility between the designed and printed structure. The G-code provisions of the designed structure and the ultimate printed product were represented in the Fig. 17. While designing/coding the given structure in Fig. 17, it has been considered load-bearing capacity and possible settlement with self-weight of consecutive layers. Otherwise, the smallest error in the code,

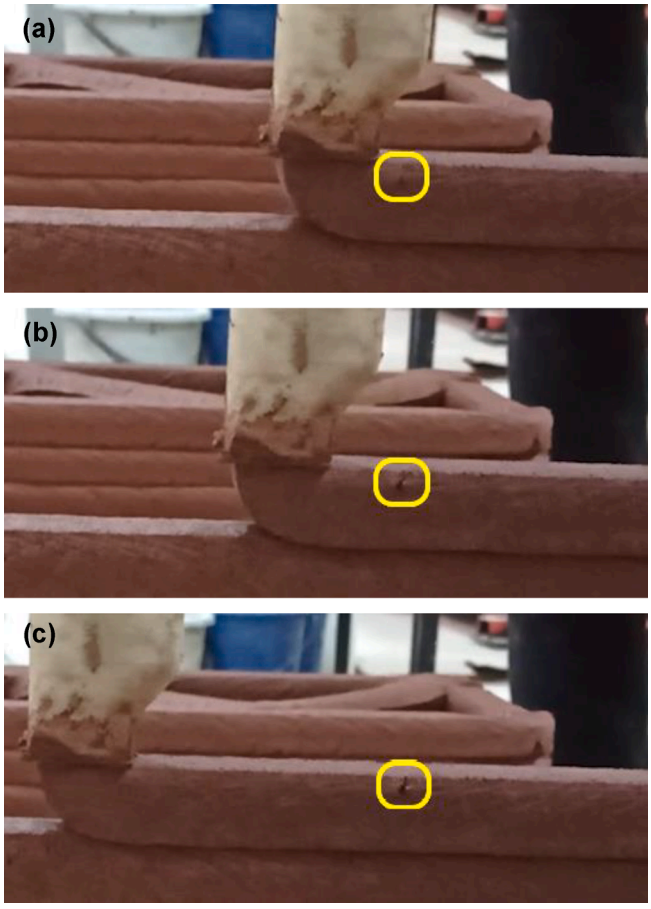

Fig. 16. Images taken during the printing operation of Mixture-A.

due to self-settlement and/or material-/printer-related discontinuity, can become significant since the number of overlapping layers or the distance to be printed along a line increases. As observed in the single- and multi-layer printed products, there were no considerable cracks/voids/fractures available on the surfaces of layered structures of ultimate product. Designed and printed structures successfully matched each other as the printed layer did not collapse or show discontinuity during manufacturing. Additionally, to have an understanding on the design capability/capacity of CDW-based mixtures with 3D-AM system, inner walls of designed structure were visually investigated to reveal whether the mixture was proper for fine workmanship that requires the

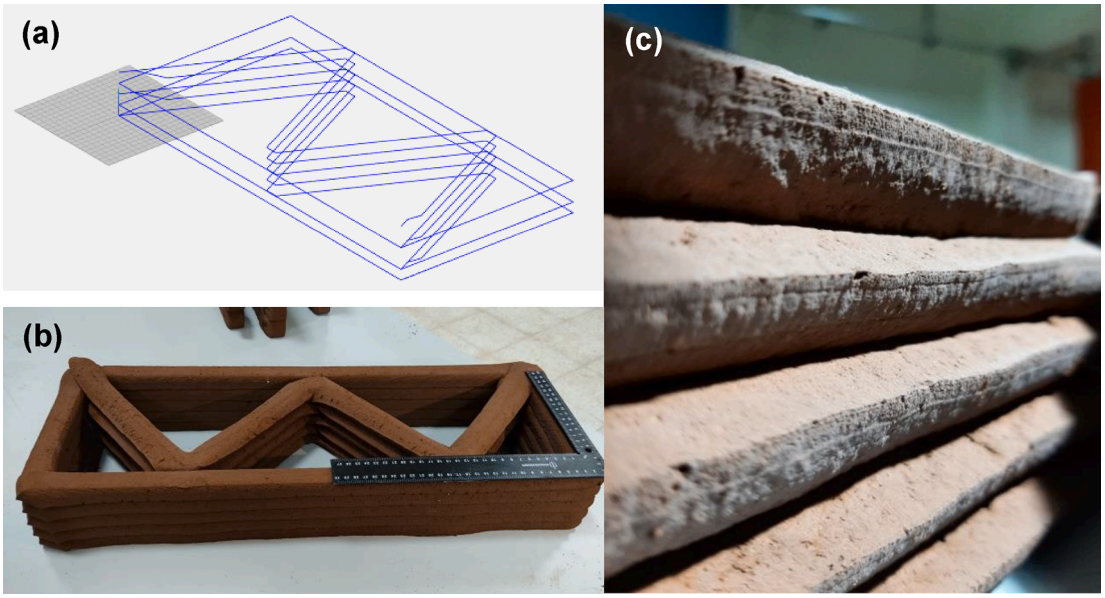

Fig. 17. Images of 3D printed structure of Mixture-A (a) provision of the G-code of the designed structure on software, (b) view of 3D-printed structure, (c) close-up view of the printed layers.

high shape retention. As seen from Fig. 17, sharp corners/edges of the printed structure obtained without any structural disorder. The most remarkable part of this situation is the elimination of architectural design constraints arising from material and formwork systems thanks to the ability of layered structure to retain its shape under burden of consecutive layers without any support. Consequently, the designed 100% CDW-based geopolymer mortars without any rheology modifying admixtures were shown to be capable of extrusion via 3D-AM free of any defects/discontinuity and fully matched with the designed structure.

4. Conclusions

This paper investigated the rheological properties of entirely CDW-based geopolymer mortar mixtures without any chemical admixtures by performing empirical tests, including flow table, buildability, and vane shear and their suitability for 3D-AM purposes via printing applications made by a laboratory-scale 3D printer. Capability of the empirical test methods in determining the suitability of the mixtures for 3D-AM purposes was investigated, along with the effects of alkaline activators on the rheology and compressive strength of the mixtures. Following conclusions have been drawn from the experimental works:.

- Single use of NaOH at different molarities was influential on the rheological properties with a clear trend that was inverted at a certain level of molarity (10 M−NaOH). While flowability was enhanced up to 10 M, the trend reversed after this level, and a similar trend was observed for the buildability and vane shear stress results with an opposite behavior. Time-dependent empirical tests gave consistent and repetitive results.
- Incorporation of $Ca(OH)_2$ into the mixtures caused increment in the viscosity lowering flowability index, increasing buildability and vane shear stress results at the fresh state of the geopolymer mixtures, regardless of type/amount of activators. Considering the open-time workability performance, inclusion of $Ca(OH)_2$ had no meaningful effect on the setting behavior of the mixtures.
- Incorporation of Na_2SiO_3 into the geopolymer mortars resulted in considerable decrements in the initial yield stress of the mixtures, increasing flowability. However, this also caused a rapid hardening in less than 30 min, which means shortening of the period (open-time) for 3D printability.
- Mixtures activated by the single use of NaOH having different molarities exhibited similar 28-day compressive strength with an approximate result of 11 MPa. Incorporation of $Ca(OH)_2$ as the alkaline activator led increments in the 28-day compressive strength of the mixtures with an approximate result of 17.9 MPa. With the addition of Na_2SiO_3 into the mixtures containing $Ca(OH)_2$ and NaOH, 28-day compressive strength as well as the strength development rate was significantly improved reaching to an approximate result of 36 MPa.
- Recycled concrete aggregates can be used in CDW-based systems without endangering the rheological properties and compressive strength of the mixtures suitable for 3D-AM.
- The printability of entirely CDW-based geopolymer mortars without any chemical admixtures was shown clearly via 3D-AM process almost free of any defects/discontinuity. End products obtained from two separate mixtures having high and low viscosity showed that empirical test methods used herein were capable of evaluating the performance of the mixtures in regard to parameters important for 3D-AM including printability, flowability, viscosity, buildability, extrudability and open-time. Overall, printed final product with mortar mixture having a low viscosity is perfectly matched with the G-code of the designed structure, dimensionally.
- Buildability test results obtained from empirical test were overlapped with the performance of 3D printed final product regarding final height of designed structures. Empirical buildability performance assessment is therefore considered as proper method to predict the performance of 3D-AM final layered structure.

In the current work, the type/content of CDW-based precursors were kept constant based on the previous experience of the authors and the main focus was placed on the detailed effects of type/content of alkaline activators on the rheological properties and compressive strength of geopolymer mortars suitable for 3D-AM. However, it is of importance to finally note that the outcomes are very likely to be different in the presence of different type/content of precursors, which can be an attractive subject for further future works.

Declaration of Competing Interest

The authors declare that they have no known competing financial

interests or personal relationships that could have appeared to influence the work reported in this paper.

Acknowledgement

The authors gratefully acknowledge the financial assistance of the Scientific and Technical Research Council (TUBITAK) of Turkey provided under Project: 119M630 and 119N030.

References

[1] P.J. Monteiro, S.A. Miller, A. Horvath, Towards sustainable concrete, Nature materials 16 (7) (2017) 698–699, https://doi.org/10.1038/nmat4930.
[2] A. Josa, A. Aguado, A. Cardim, E. Byars, Comparative analysis of the life cycle impact assessment of available cement inventories in the EU, Cement and Concrete Research 37 (5) (2007) 781–788, https://doi.org/10.1016/j.cemconres.2007.02.004.
[3] U.s. Environmental Protection Agency (EPA), Advancing sustainable materials management 2015 2014 fact sheet.
[4] AECOM, Asia Company Limited. People's Republic of China: Construction and Demolition Waste Management and Recycling., (2018).
[5] Urban Transformation Action Plan, Republic of Turkey Ministry of Environment and Urbanization, (2019).
[6] X. Guo, H. Shi, L. Chen, W.A. Dick, Alkali-activated complex binders from class C fly ash and Ca-containing admixtures, Journal of Hazardous Materials 173 (1–3) (2010) 480–486, https://doi.org/10.1016/j.jhazmat.2009.08.110.
[7] J.L. Provis, Alkali-activated materials, Cement and Concrete Research 114 (2018) 40–48, https://doi.org/10.1016/j.cemconres.2017.02.009.
[8] H. Ulugöl, A. Kul, G. Yıldırım, M. Şahmaran, A. Aldemir, D. Figueira, A. Ashour, Mechanical and microstructural characterization of geopolymers from assorted construction and demolition waste-based masonry and glass, Journal of Cleaner Production 280 (2021), 124358, https://doi.org/10.1016/j.jclepro.2020.124358.
[9] S. Dadsetan, H. Siad, M. Lachemi, M. Sahmaran, Construction and demolition waste in geopolymer concrete technology: a review, Magazine of Concrete Research 71 (23) (2019) 1232–1252, https://doi.org/10.1680/jmacr.18.00307.
[10] B. Khoshnevis, Automated construction by contour crafting—related robotics and information technologies, Automation in construction 13 (1) (2004) 5–19, https://doi.org/10.1016/j.autcon.2003.08.012.
[11] V. Nerella, M. Krause, M. Näther, V. Mechtcherine, 3D printing technology for on-site construction, CPI-Concr. Plant Int 4 (2016) 36–41.
[12] T. Wangler, E. Lloret, L. Reiter, N. Hack, F. Gramazio, M. Kohler, M. Bernhard, B. Dillenburger, J. Buchli, N. Roussel, Digital concrete: opportunities and challenges, RILEM Technical Letters 1 (2016) 67–75, https://doi.org/10.21809/rilemtechlett.2016.16.
[13] N. Hopkinson, Y. Gao, D. McAfee, Design for environment analyses applied to rapid manufacturing, Proceedings of the Institution of Mechanical Engineers, Part D: Journal of Automobile Engineering 220 (10) (2006) 1363–1372, https://doi.org/10.1243/09544070JAUTO309.
[14] R.A. Buswell, R.C. Soar, A.G. Gibb, A. Thorpe, Freeform construction: mega-scale rapid manufacturing for construction, Automation in construction 16 (2) (2007) 224–231, https://doi.org/10.1016/j.autcon.2006.05.002.
[15] B. Panda, S.C. Paul, L.J. Hui, Y.W.D. Tay, M.J. Tan, Additive manufacturing of geopolymer for sustainable built environment, Journal of cleaner production 167 (2017) 281–288, https://doi.org/10.1016/j.jclepro.2017.08.165.
[16] B. Panda, S.C. Paul, N.A.N. Mohamed, Y.W.D. Tay, M.J. Tan, Measurement of tensile bond strength of 3D printed geopolymer mortar, Measurement 113 (2018) 108–116, https://doi.org/10.1016/j.measurement.2017.08.051.
[17] B. Panda, C. Unluer, M.J. Tan, Investigation of the rheology and strength of geopolymer mixtures for extrusion-based 3D printing, Cement and Concrete Composites 94 (2018) 307–314, https://doi.org/10.1016/j.cemconcomp.2018.10.002.
[18] B. Panda, N.A.N. Mohamed, M.J. Tan, Effect of 3d printing on mechanical properties of fly ash-based inorganic geopolymer, International Congress on Polymers in Concrete, Springer (2018) 509–515, https://doi.org/10.1007/978-3-319-78175-4_65.
[19] B. Panda, N.A.N. Mohamed, Y.W.D. Tay, M.J. Tan, Bond strength in 3D printed geopolymer mortar, RILEM International Conference on Concrete and Digital Fabrication, Springer (2018) 200–206, https://doi.org/10.1007/978-3-319-99519-9_18.
[20] A. Annapareddy, B. Panda, A. Ting, M. Li, M. Tan, Flow and mechanical properties of 3D printed cementitious material with recycled glass aggregates, Proceedings of the 3rd International Conference on Progress in Additive Manufacturing (Pro-AM 2018), Singapore, 2018, pp. 14-17. https://doi.org/10.25341/D41P4H.
[21] J.H. Lim, B. Panda, Q.-C. Pham, Improving flexural characteristics of 3D printed geopolymer composites with in-process steel cable reinforcement, Construction and Building Materials 178 (2018) 32–41, https://doi.org/10.1016/j.conbuildmat.2018.05.010.
[22] B. Panda, M.J. Tan, Experimental study on mix proportion and fresh properties of fly ash based geopolymer for 3D concrete printing, Ceramics International 44 (9) (2018) 10258–10265, https://doi.org/10.1016/j.ceramint.2018.03.031.
[23] B. Nematollahi, P. Vijay, J. Sanjayan, A. Nazari, M. Xia, V. Naidu Nerella, V. Mechtcherine, Effect of polypropylene fibre addition on properties of geopolymers made by 3D printing for digital construction, Materials 11 (12) (2018) 2352, https://doi.org/10.3390/ma11122352.
[24] S.H. Bong, B. Nematollahi, A. Nazari, M. Xia, J.G. Sanjayan, Fresh and hardened properties of 3D printable geopolymer cured in ambient temperature, RILEM International Conference on Concrete and Digital Fabrication, Springer (2018) 3–11, https://doi.org/10.1007/978-3-319-99519-9_1.
[25] A. Kashani, T. Ngo, Optimisation of mixture properties for 3D printing of geopolymer concrete, ISARC. Proceedings of the International Symposium on Automation and Robotics in Construction, IAARC Publications, 2018, pp. 1-8. https://doi.org/10.22260/ISARC2018/0037.
[26] B. Panda, C. Unluer, M.J. Tan, Extrusion and rheology characterization of geopolymer nanocomposites used in 3D printing, Composites Part B: Engineering 176 (2019), 107290, https://doi.org/10.1016/j.compositesb.2019.107290.
[27] B. Panda, G.B. Singh, C. Unluer, M.J. Tan, Synthesis and characterization of one-part geopolymers for extrusion based 3D concrete printing, Journal of cleaner production 220 (2019) 610–619, https://doi.org/10.1016/j.jclepro.2019.02.185.
[28] D.-W. Zhang, D.-M. Wang, X.-Q. Lin, T. Zhang, The study of the structure rebuilding and yield stress of 3D printing geopolymer pastes, Construction and Building Materials 184 (2018) 575–580, https://doi.org/10.1016/j.conbuildmat.2018.06.233.
[29] C. Sun, J. Xiang, M. Xu, Y. He, Z. Tong, X. Cui, 3D extrusion free forming of geopolymer composites: Materials modification and processing optimization, Journal of Cleaner Production 258 (2020), 120986, https://doi.org/10.1016/j.jclepro.2020.120986.
[30] H. Alghamdi, N. Neithalath, Synthesis and characterization of 3D-printable geopolymeric foams for thermally efficient building envelope materials, Cement and Concrete Composites 104 (2019), 103377, https://doi.org/10.1016/j.cemconcomp.2019.103377.
[31] M. Xia, J.G. Sanjayan, Methods of enhancing strength of geopolymer produced from powder-based 3D printing process, Materials Letters 227 (2018) 281–283, https://doi.org/10.1016/j.matlet.2018.05.100.
[32] Z. Li, L. Wang, G. Ma, Mechanical improvement of continuous steel microcable reinforced geopolymer composites for 3D printing subjected to different loading conditions, Composites Part B: Engineering 187 (2020), 107796, https://doi.org/10.1016/j.compositesb.2020.107796.
[33] G. Ma, Z. Li, L. Wang, G. Bai, Micro-cable reinforced geopolymer composite for extrusion-based 3D printing, Materials Letters 235 (2019) 144–147, https://doi.org/10.1016/j.matlet.2018.09.159.
[34] B. Nematollahi, M. Xia, J. Sanjayan, P. Vijay, Effect of type of fiber on inter-layer bond and flexural strengths of extrusion-based 3D printed geopolymer, Materials science forum, Trans Tech Publ (2018) 155–162, https://doi.org/10.4028/www.scientific.net/MSF.939.155.
[35] B. Nematollahi, M. Xia, S.H. Bong, J. Sanjayan, Hardened properties of 3D printable 'one-part'geopolymer for construction applications, RILEM International Conference on Concrete and Digital Fabrication, Springer (2018) 190–199, https://doi.org/10.1007/978-3-319-99519-9_17.
[36] S. Al-Qutaifi, A. Nazari, A. Bagheri, Mechanical properties of layered geopolymer structures applicable in concrete 3D-printing, Construction and Building Materials 176 (2018) 690–699, https://doi.org/10.1016/j.conbuildmat.2018.04.195.
[37] B. Panda, S.C. Paul, M.J. Tan, Anisotropic mechanical performance of 3D printed fiber reinforced sustainable construction material, Materials Letters 209 (2017) 146–149, https://doi.org/10.1016/j.matlet.2017.07.123.
[38] O. Şahin, H. İlcan, A.T. Ateşli, A. Kul, G. Yıldırım, M. Şahmaran, Construction and demolition waste-based geopolymers suited for use in 3-dimensional additive manufacturing, Cement and Concrete Composites 121 (2021), 104088, https://doi.org/10.1016/j.cemconcomp.2021.104088.
[39] H. Ye, Y. Zhang, Z. Yu, Wood flour's effect on the properties of geopolymer-based composites at different curing times, BioResources 13 (2) (2018) 2499–2514.
[40] A. Bouaissi, L.Y. Li, L.M. Moga, I.G. Sandu, M. Abdullah, A.V. Sandu, A review on fly ash as a raw cementitious material for geopolymer concrete, Rev. Chim 69 (7) (2018), https://doi.org/10.37358/RC.18.7.6390.
[41] W. Zailani, M. Abdullah, M. Arshad, D. Burduhos-Nergis, M. Tahir, Effect of Iron Oxide (Fe2O3) on the Properties of Fly Ash Based Geopolymer, IOP Conference Series: Materials Science and Engineering, IOP Publishing (2020), 012017, https://doi.org/10.1088/1757-899X/877/1/012017.
[42] N.H. Thang, Evaluation on Formation of Aluminosilicate Network in Ternary-Blended Geopolymer Using Infrared Spectroscopy, Solid State Phenomena, Trans Tech Publ (2019) 99–104, https://doi.org/10.4028/www.scientific.net/SSP.296.99.
[43] O.K. Wattimena, D.H. Antoni, A review on the effect of fly ash characteristics and their variations on the synthesis of fly ash based geopolymer, AIP Conference Proceedings, AIP Publishing LLC (2017), 020041, https://doi.org/10.1063/1.5003524.
[44] A. Kazemian, X. Yuan, E. Cochran, B. Khoshnevis, Cementitious materials for construction-scale 3D printing: Laboratory testing of fresh printing mixture, Construction and Building Materials 145 (2017) 639–647, https://doi.org/10.1016/j.conbuildmat.2017.04.015.
[45] Y.Y. Kim, H.-J. Kong, V.C. Li, Design of engineered cementitious composite suitable for wet-mixture shotcreting, Materials Journal 100 (6) (2003) 511–518, https://doi.org/10.14359/12958.
[46] K. Khayat, A. Omran, S. Neji, P. Billberg, A. Yahia, Test methods to evaluate form pressure of SCC, Proceedings of the 3rd North American Conference on the Design and Use of Self-Consolidating Concrete (SCC 2008), Chicago, IL, 2008, pp. 308-314.

[47] M.A. Abd Elaty, M.F. Ghazy, Flow properties of fresh concrete by using modified geotechnical vane shear test, HBRC journal 8(3) (2012) 159-169. https://doi.org/10.1016/j.hbrcj.2012.07.001.
[48] Astm, C109 / C109M–20b, Cement, Standard test method for compressive strength of hydraulic cement mortars (using 2-in. or [50-mm] cube specimens), ASTM, International (2016).
[49] D.-W. Zhang, D.-M. Wang, Z. Liu, F.-Z. Xie, Rheology, agglomerate structure, and particle shape of fresh geopolymer pastes with different NaOH activators content, Construction and Building Materials 187 (2018) 674–680, https://doi.org/10.1016/j.conbuildmat.2018.07.205.
[50] V. Glukhovsky, Soil silicate articles and structures, Russian, Budivel'nyk Publish, Kiev, 1967.
[51] K. Vance, A. Dakhane, G. Sant, N. Neithalath, Observations on the rheological response of alkali activated fly ash suspensions: the role of activator type and concentration, Rheologica Acta 53 (10–11) (2014) 843–855, https://doi.org/10.1007/s00397-014-0793-z.
[52] D. Khale, R. Chaudhary, Mechanism of geopolymerization and factors influencing its development: a review, Journal of materials science 42 (3) (2007) 729–746, https://doi.org/10.1007/s10853-006-0401-4.
[53] S.V. Patankar, Y.M. Ghugal, S.S. Jamkar, Effect of concentration of sodium hydroxide and degree of heat curing on fly ash-based geopolymer mortar, Indian Journal of Materials Science 2014 (2014), https://doi.org/10.1155/2014/938789.
[54] Y. Rifaai, A. Yahia, A. Mostafa, S. Aggoun, E.-H. Kadri, Rheology of fly ash-based geopolymer: Effect of NaOH concentration, Construction and Building Materials 223 (2019) 583–594, https://doi.org/10.1016/j.conbuildmat.2019.07.028.
[55] G.F. Huseien, M. Ismail, N.H.A. Khalid, M.W. Hussin, J. Mirza, Compressive strength and microstructure of assorted wastes incorporated geopolymer mortars: Effect of solution molarity, Alexandria engineering journal 57 (4) (2018) 3375–3386, https://doi.org/10.1016/j.aej.2018.07.011.
[56] S. Alonso, A. Palomo, Alkaline activation of metakaolin and calcium hydroxide mixtures: influence of temperature, activator concentration and solids ratio, Materials Letters 47 (1–2) (2001) 55–62, https://doi.org/10.1016/S0167-577X(00)00212-3.
[57] Y.-M. Liew, C.-Y. Heah, H. Kamarudin, Structure and properties of clay-based geopolymer cements: A review, Progress in Materials Science 83 (2016) 595–629, https://doi.org/10.1016/j.pmatsci.2016.08.002.
[58] J. Feng, R. Zhang, L. Gong, Y. Li, W. Cao, X. Cheng, Development of porous fly ash-based geopolymer with low thermal conductivity, Materials & Design (1980-2015) 65 (2015) 529-533. https://doi.org/10.1016/j.matdes.2014.09.024.
[59] J.L. Provis, J.S.J. Van Deventer, Geopolymers: structures, processing, properties and industrial applications, Elsevier, 2009.
[60] H.A. Gasteiger, W.J. Frederick, R.C. Streisel, Solubility of aluminosilicates in alkaline solutions and a thermodynamic equilibrium model, Industrial & engineering chemistry research 31 (4) (1992) 1183–1190.
[61] G. Görhan, G. Kürklü, The influence of the NaOH solution on the properties of the fly ash-based geopolymer mortar cured at different temperatures, Composites part b: engineering 58 (2014) 371–377, https://doi.org/10.1016/j.compositesb.2013.10.082.
[62] M.L. Granizo, S. Alonso, M.T. Blanco-Varela, A. Palomo, Alkaline activation of metakaolin: effect of calcium hydroxide in the products of reaction, Journal of the American Ceramic Society 85 (1) (2002) 225–231, https://doi.org/10.1111/j.1151-2916.2002.tb00070.x.
[63] A. Fernández-Jiménez, A. Palomo, M. Criado, Microstructure development of alkali-activated fly ash cement: a descriptive model, Cement and concrete research 35 (6) (2005) 1204–1209, https://doi.org/10.1016/j.cemconres.2004.08.021.
[64] B. Akturk, A.B. Kizilkanat, N. Kabay, Effect of calcium hydroxide on fresh state behavior of sodium carbonate activated blast furnace slag pastes, Construction and Building Materials 212 (2019) 388–399, https://doi.org/10.1016/j.conbuildmat.2019.03.328.
[65] H. Khater, Effect of calcium on geopolymerization of aluminosilicate wastes, Journal of materials in civil engineering 24 (1) (2012) 92–101, https://doi.org/10.1061/(ASCE)MT.1943-5533.0000352.
[66] X. Chen, A. Sutrisno, L.J. Struble, Effects of calcium on setting mechanism of metakaolin-based geopolymer, Journal of the American Ceramic Society 101 (2) (2018) 957–968, https://doi.org/10.1111/jace.15249.
[67] J. Temuujin, A. Van Riessen, R. Williams, Influence of calcium compounds on the mechanical properties of fly ash geopolymer pastes, Journal of hazardous materials 167 (1–3) (2009) 82–88, https://doi.org/10.1016/j.jhazmat.2008.12.121.
[68] C.K. Yip, G. Lukey, J.S. Van Deventer, The coexistence of geopolymeric gel and calcium silicate hydrate at the early stage of alkaline activation, Cement and concrete research 35 (9) (2005) 1688–1697, https://doi.org/10.1016/j.cemconres.2004.10.042.
[69] S. Puligilla, P. Mondal, Role of slag in microstructural development and hardening of fly ash-slag geopolymer, Cement and concrete Research 43 (2013) 70–80, https://doi.org/10.1016/j.cemconres.2012.10.004.
[70] J. Davidovits, Geopolymers: inorganic polymeric new materials, Journal of Thermal Analysis and calorimetry 37 (8) (1991) 1633–1656, https://doi.org/10.1007/bf01912193.
[71] X. Guo, H. Shi, Metakaolin-, fly ash-and calcium hydroxide-based geopolymers: effects of calcium on performance, Advances in Cement Research 27 (10) (2015) 559–566, https://doi.org/10.1680/adcr.14.00081.
[72] C. Li, H. Sun, L. Li, A review: The comparison between alkali-activated slag (Si+ Ca) and metakaolin (Si+ Al) cements, Cement and concrete research 40 (9) (2010) 1341–1349, https://doi.org/10.1016/j.cemconres.2010.03.020.
[73] A. Favier, J. Hot, G. Habert, N. Roussel, J.-B.d.E. de Lacaillerie, Flow properties of MK-based geopolymer pastes. A comparative study with standard Portland cement pastes, Soft Matter 10(8) (2014) 1134-1141. https://doi.org/10.1039/C3SM51889B.
[74] H.Y. Leong, D.E.L. Ong, J.G. Sanjayan, A. Nazari, The effect of different Na2O and K2O ratios of alkali activator on compressive strength of fly ash based-geopolymer, Construction and Building Materials 106 (2016) 500–511, https://doi.org/10.1016/j.conbuildmat.2015.12.141.
[75] H.H. Weldes, K.R. Lange, Properties of soluble silicates, Industrial & Engineering Chemistry 61 (4) (1969) 29–44.
[76] A. Kashani, J.L. Provis, G.G. Qiao, J.S. van Deventer, The interrelationship between surface chemistry and rheology in alkali activated slag paste, Construction and Building Materials 65 (2014) 583–591, https://doi.org/10.1016/j.conbuildmat.2014.04.127.
[77] M. Palacios, M. Alonso, C. Varga, F. Puertas, Influence of the alkaline solution and temperature on the rheology and reactivity of alkali-activated fly ash pastes, Cement and Concrete Composites 95 (2019) 277–284, https://doi.org/10.1016/j.cemconcomp.2018.08.010.
[78] K. Kondepudi, K.V. Subramaniam, Rheological characterization of low-calcium fly ash suspensions in alkaline silicate colloidal solutions for geopolymer concrete production, Journal of Cleaner Production 234 (2019) 690–701, https://doi.org/10.1016/j.jclepro.2019.06.124.
[79] G. Landrou, C. Brumaud, F. Winnefeld, R.J. Flatt, G. Habert, Lime as an anti-plasticizer for self-compacting clay concrete, Materials 9 (5) (2016) 330, https://doi.org/10.3390/ma9050330.
[80] A.R. Kotwal, Y.J. Kim, J. Hu, V. Sriraman, Characterization and early age physical properties of ambient cured geopolymer mortar based on class C fly ash, International Journal of Concrete Structures and Materials 9 (1) (2015) 35–43, https://doi.org/10.1007/s40069-014-0085-0.
[81] S. Goberis, V. Antonovich, Influence of sodium silicate amount on the setting time and EXO temperature of a complex binder consisting of high-aluminate cement, liquid glass and metallurgical slag, Cement and concrete research 34 (10) (2004) 1939–1941, https://doi.org/10.1016/j.cemconres.2004.01.004.
[82] M. Criado, A. Palomo, A. Fernández-Jiménez, Alkali activation of fly ashes. Part 1: Effect of curing conditions on the carbonation of the reaction products, Fuel 84(16) (2005) 2048-2054. https://doi.org/10.1016/j.fuel.2005.03.030.
[83] A. Fernández-Jiménez, F. Puertas, Effect of activator mix on the hydration and strength behaviour of alkali-activated slag cements, Advances in cement research 15 (3) (2003) 129–136, https://doi.org/10.1680/adcr.2003.15.3.129.
[84] C. Shi, R.L. Day, A calorimetric study of early hydration of alkali-slag cements, Cement and concrete Research 25 (6) (1995) 1333–1346, https://doi.org/10.1016/0008-8846(95)00126-W.
[85] A. Mustafa Al Bakri, H. Kamarudin, M. Bnhussain, A. Rafiza, Y. Zarina, Effect of Na 2 SiO 3/NaOH Ratios and NaOH Molarities on Compressive Strength of Fly-Ash-Based Geopolymer, ACI Materials Journal 109(5) (2012). https://doi.org/10.14359/51684080.
[86] T. Phoo-ngernkham, A. Maegawa, N. Mishima, S. Hatanaka, P. Chindaprasirt, Effects of sodium hydroxide and sodium silicate solutions on compressive and shear bond strengths of FA–GBFS geopolymer, Construction and Building Materials 91 (2015) 1–8, https://doi.org/10.1016/j.conbuildmat.2015.05.001.
[87] P. Risdanareni, J.J. Ekaputri, The influence of alkali activator concentration to mechanical properties of geopolymer concrete with trass as a filler, Materials Science Forum, Trans Tech Publ (2015) 125–134, https://doi.org/10.4028/www.scientific.net/MSF.803.125.
[88] B. De Jong, G.E. Brown Jr, Polymerization of silicate and aluminate tetrahedra in glasses, melts, and aqueous solutions—I. Electronic structure of H6Si2O7, H6AlSiO71−, and H6Al2O72−, Geochimica et Cosmochimica Acta 44(3) (1980) 491–511, https://doi.org/10.1016/0016-7037(80)90046-0.
[89] A.M.M. Al Bakri, O. Kareem, S. Myint, Study on the effect of alkaline activators ratio in preparation of fly ash-based geopolymer, (2009).
[90] P. Duxson, J.L. Provis, G.C. Lukey, S.W. Mallicoat, W.M. Kriven, J.S. Van Deventer, Understanding the relationship between geopolymer composition, microstructure and mechanical properties, Colloids and Surfaces A: Physicochemical and Engineering Aspects 269 (1–3) (2005) 47–58, https://doi.org/10.1016/j.colsurfa.2005.06.060.
[91] S. Yaseri, G. Hajiaghaei, F. Mohammadi, M. Mahdikhani, R. Farokhzad, The role of synthesis parameters on the workability, setting and strength properties of binary binder based geopolymer paste, Construction and Building Materials 157 (2017) 534–545, https://doi.org/10.1016/j.conbuildmat.2017.09.102.
[92] M. Komljenović, Z. Baščarević, V. Bradić, Mechanical and microstructural properties of alkali-activated fly ash geopolymers, Journal of Hazardous Materials 181 (1–3) (2010) 35–42, https://doi.org/10.1016/j.jhazmat.2010.04.064.
[93] G. Kovalchuk, A. Fernández-Jiménez, A. Palomo, Alkali-activated fly ash: effect of thermal curing conditions on mechanical and microstructural development–Part II, Fuel 86 (3) (2007) 315–322, https://doi.org/10.1016/j.fuel.2006.07.010.
[94] G.S. Ryu, Y.B. Lee, K.T. Koh, Y.S. Chung, The mechanical properties of fly ash-based geopolymer concrete with alkaline activators, Construction and building materials 47 (2013) 409–418, https://doi.org/10.1016/j.conbuildmat.2013.05.069.
[95] G. Yıldırım, A. Kul, E. Özçelikci, M. Şahmaran, A. Aldemir, D. Figueira, A. Ashour, Development of alkali-activated binders from recycled mixed masonry-originated waste, Journal of Building Engineering 33 (2021), 101690, https://doi.org/10.1016/j.jobe.2020.101690.
[96] L. Evangelista, J. de Brito, Mechanical behaviour of concrete made with fine recycled concrete aggregates, Cement and concrete composites 29 (5) (2007) 397–401, https://doi.org/10.1016/j.cemconcomp.2006.12.004.

[97] M.B. Leite, J.G.L.F. do Filho, P.R. Lima, Workability study of concretes made with recycled mortar aggregate, Materials and structures 46(10) (2013) 1765-1778. https://doi.org/10.1617/s11527-012-0010-4.
[98] G. Tabilo-Munizaga, G.V. Barbosa-Cánovas, Rheology for the food industry, Journal of food engineering 67 (1–2) (2005) 147–156, https://doi.org/10.1016/j.jfoodeng.2004.05.062.
[99] K. Komnitsas, D. Zaharaki, A. Vlachou, G. Bartzas, M. Galetakis, Effect of synthesis parameters on the quality of construction and demolition wastes (CDW) geopolymers, Advanced Powder Technology 26 (2) (2015) 368–376, https://doi.org/10.1016/j.apt.2014.11.012.